Electronic Supplementary Material (ESI) for Dalton Transactions

Dalton Transactions

Electronic Supplementary Information

Synthesis, structure and spectroscopic properties of Re(I) complexes incorporating 5-arylazo-8-hydroxyquinoline: a density functional theory/time dependent density functional theory investigation

Rupa Sarkar, Pallab Mondal, and Kajal Krishna Rajak[*]

Inorganic Chemistry Section, Department of Chemistry, Jadavpur University, Kolkata,
700 032, India

[*] To whom correspondence should be addressed. Email: kajalrajak@hotmail.com

Jadavpur University

Table S1 Selected optimized geometrical parameters for $[Re_2(CO)_6(hq^2)_2]$, **2;** $[Re(CO)_3(hq^2)(Im)]$, **2a** and $[Re(CO)_3(hq^2)(N\text{-}MeIm)]$, **2b** in the ground **(S_0)** and lowest lying triplet **(T_1)** excited states at B3LYP levels

Bond lengths (Å)

	2			**2a**		**2b**	
	S_0	T_1		S_0	T_1	S_0	T_1
Re1–C1	1.903	1.904	Re1–C1	1.921	1.921	1.922	1.922
Re1–C2	1.905	1.905	Re1–C2	1.907	1.907	1.907	1.907
Re1–C3	1.927	1.927	Re1–C3	1.921	1.922	1.921	1.921
Re1–N1	2.211	2.210	Re1–N1	2.204	2.203	2.204	2.204
Re1–O4	2.194	2.194	Re1–N2	2.206	2.208	2.204	2.206
Re1–O4A	2.233	2.231	Re1–O4	2.156	2.155	2.156	2.155
C7–N2	1.410	1.359	C7–N4	1.401	1.355	1.400	1.356
C13–N3	1.420	1.372	C16–N5	1.419	1.371	1.419	1.371
N2–N3	1.284	1.317	N4–N5	1.287	1.338	1.287	1.339

Bond angles (°)

	2			**2a**		**2b**	
	S_0	T_1		S_0	T_1	S_0	T_1
C1–Re1–O4A	171.197	171.208	C1–Re1–N2	175.427	175.543	175.299	175.428
C2–Re1–O4	167.637	167.693	C2–Re1–O4	173.715	173.650	173.569	173.731
C3–Re1–N1	175.168	175.209	C3–Re1–N1	170.721	170.835	170.865	170.797

Dihedral angle (°)

	2			**2a**		**2b**	
	S_0	T_1		S_0	T_1	S_0	T_1
C7–N2–N3–C13	177.666	117.566	C7–N4–N5–C16	179.874	110.179	179.856	109.950

Table S2 Selected optimized geometrical parameters for [Re$_2$(CO)$_6$(hq3)$_2$], **3**; [Re(CO)$_3$(hq^3)(Im)], **3a** and [Re(CO)$_3$(hq^3)(N-MeIm)], **3b** in the ground **(S$_0$)** and lowest lying triplet **(T$_1$)** excited states at B3LYP levels

Bond lengths (Å)							
	3			**3a**		**3b**	
	S$_0$	T$_1$		S$_0$	T$_1$	S$_0$	T$_1$
Re1–C1	1.903	1.906	Re1–C1	1.922	1.921	1.922	1.922
Re1–C2	1.905	1.901	Re1–C2	1.907	1.908	1.907	1.907
Re1–C3	1.928	1.935	Re1–C3	1.922	1.921	1.921	1.921
Re1–N1	2.210	2.212	Re1–N1	2.204	2.203	2.204	2.204
Re1–O4	2.193	2.201	Re1–N2	2.206	2.207	2.205	2.206
Re1–O4A	2.235	2.239	Re1–O4	2.156	2.155	2.157	2.154
C7–N2	1.411	1.356	C7–N4	1.403	1.355	1.402	1.356
C13–N3	1.419	1.380	C16–N5	1.419	1.381	1.420	1.381
N2–N3	1.285	1.311	N4–N5	1.287	1.340	1.287	1.340
Bond angles (°)							
	3			**3a**		**3b**	
	S$_0$	T$_1$		S$_0$	T$_1$	S$_0$	T$_1$
C1–Re1–O4A	171.211	170.900	C1–Re1–N2	175.484	175.449	175.449	175.523
C2–Re1–O4	167.803	166.791	C2–Re1–O4	173.610	173.790	173.509	173.762
C3–Re1–N1	175.195	175.598	C3–Re1–N1	170.858	170.785	170.943	170.800
Dihedral angle (°)							
	3			**3a**		**3b**	
	S$_0$	T$_1$		S$_0$	T$_1$	S$_0$	T$_1$
C7–N2–N3–C13	179.901	122.554	C7–N4–N5–C16	179.651	109.688	179.918	107.580

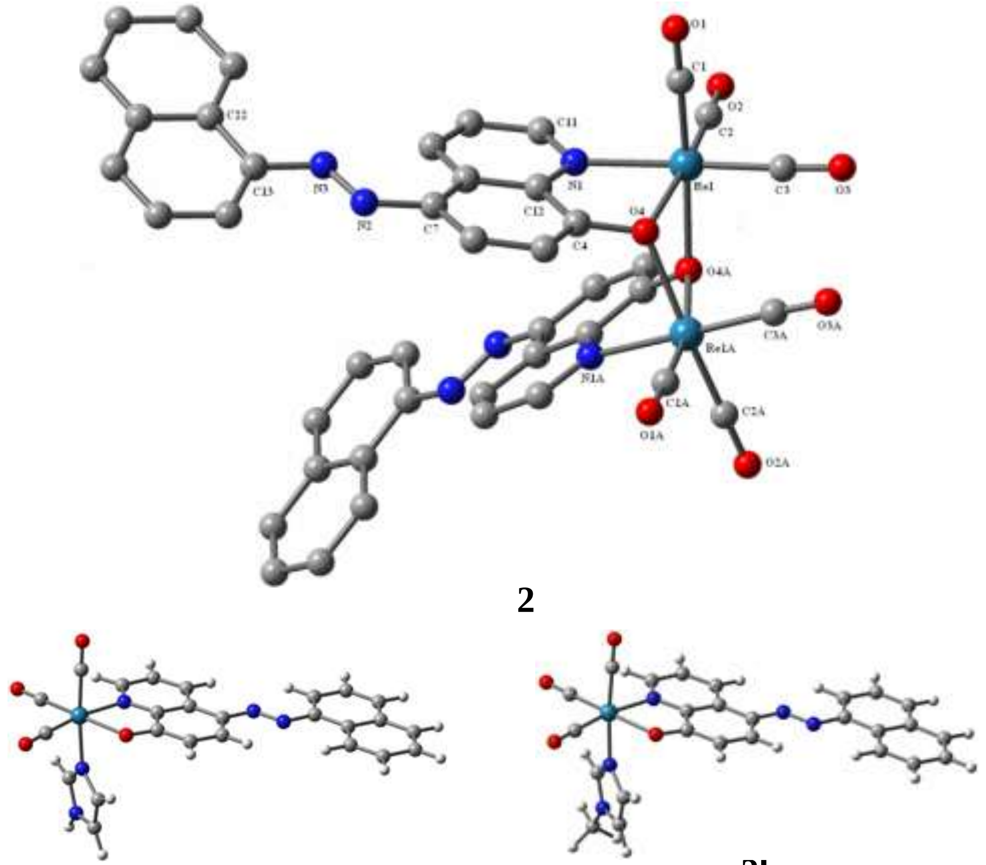

2

2a

2b

Fig. S1 Optimized molecular structures of [Re$_2$(CO)$_6$(hq^2)$_2$], **2**; [Re(CO)$_3$(hq^2)(Im)], **2a** and [Re(CO)$_3$(hq^2)(N-MeIm)], **2b** at S$_0$ state. (Re: Cyan, N: Blue, O: Red, C: Grey, H: White. All hydrogen atoms of **2** are omitted for clarity).

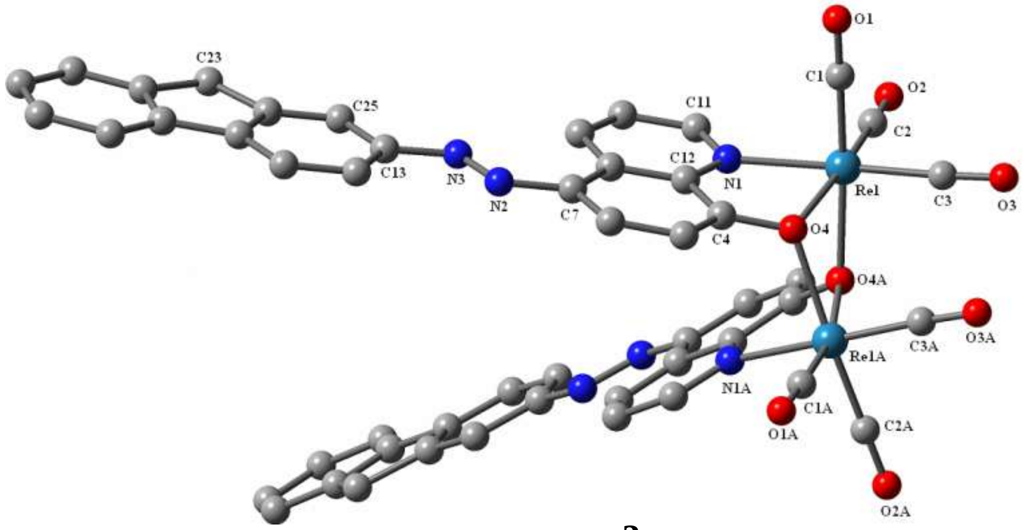

3

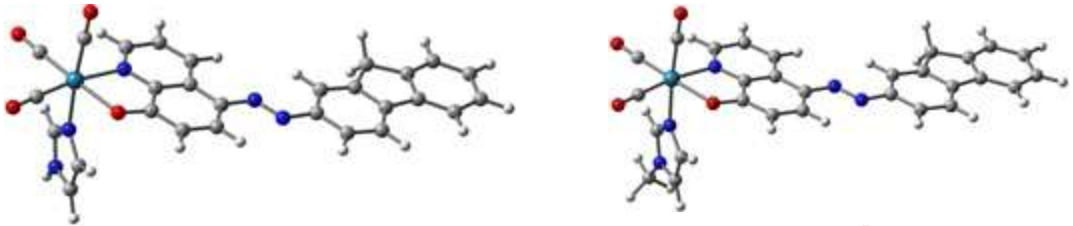

3a

3b

Fig. S2 Optimized molecular structures of [$Re_2(CO)_6(hq^3)_2$], **3**; [$Re(CO)_3(hq^3)(Im)$], **3a** and [$Re(CO)_3(hq^3)$(N-MeIm)], **3b** at S_0 state. (Re: Cyan, N: Blue, O: Red, C: Grey, H: White. All hydrogen atoms of **3** are omitted for clarity).

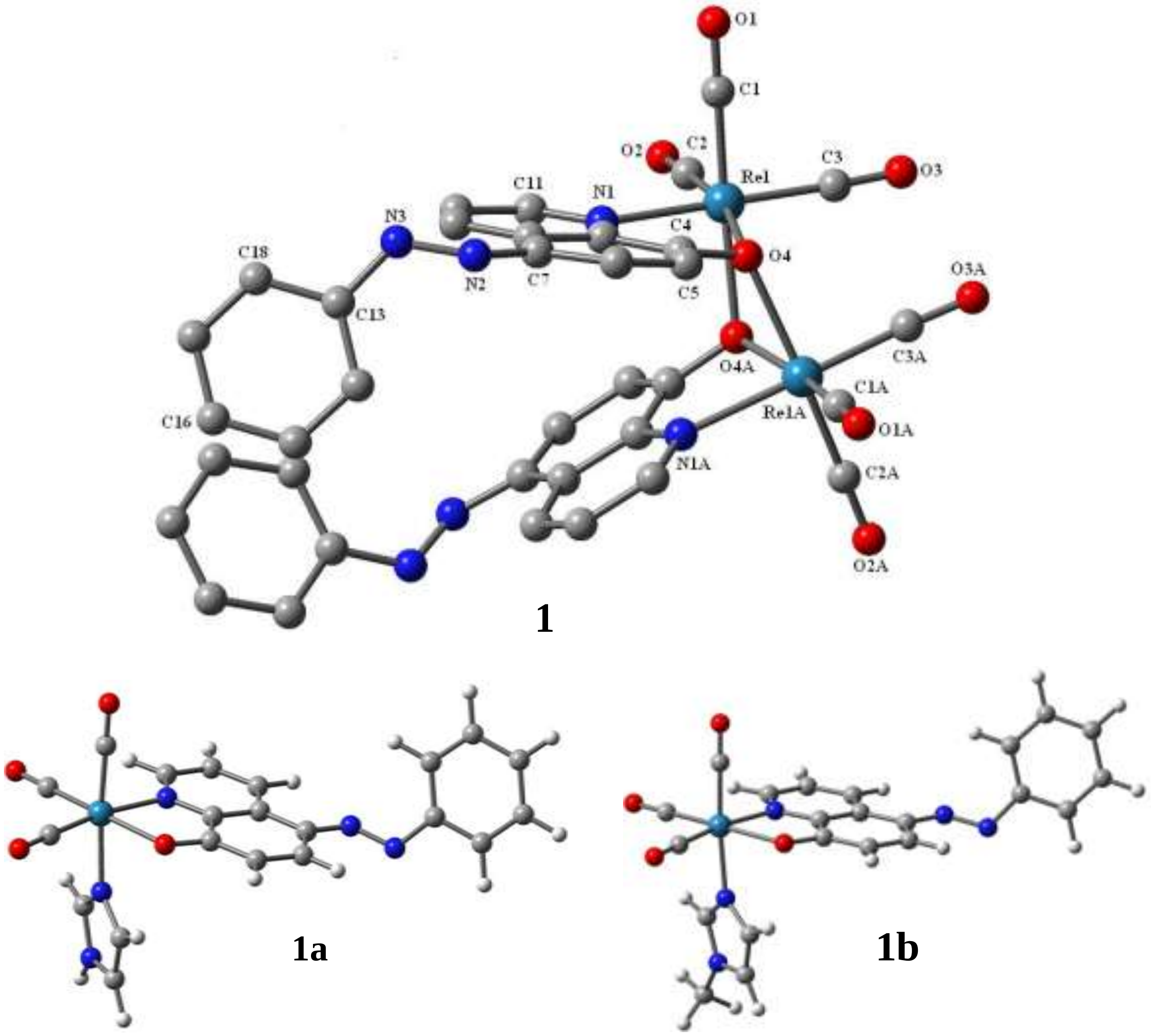

1

1a

1b

Fig. S3 Optimized molecular structures of [$Re_2(CO)_6(hq^1)_2$], **1**; [$Re(CO)_3(hq^1)(Im)$], **1a** and [$Re(CO)_3(hq^1)$(N-MeIm)], **1b** at T_1 state. (Re: Cyan, N: Blue, O: Red, C: Grey, H: White. All hydrogen atoms of **1** are omitted for clarity).
]

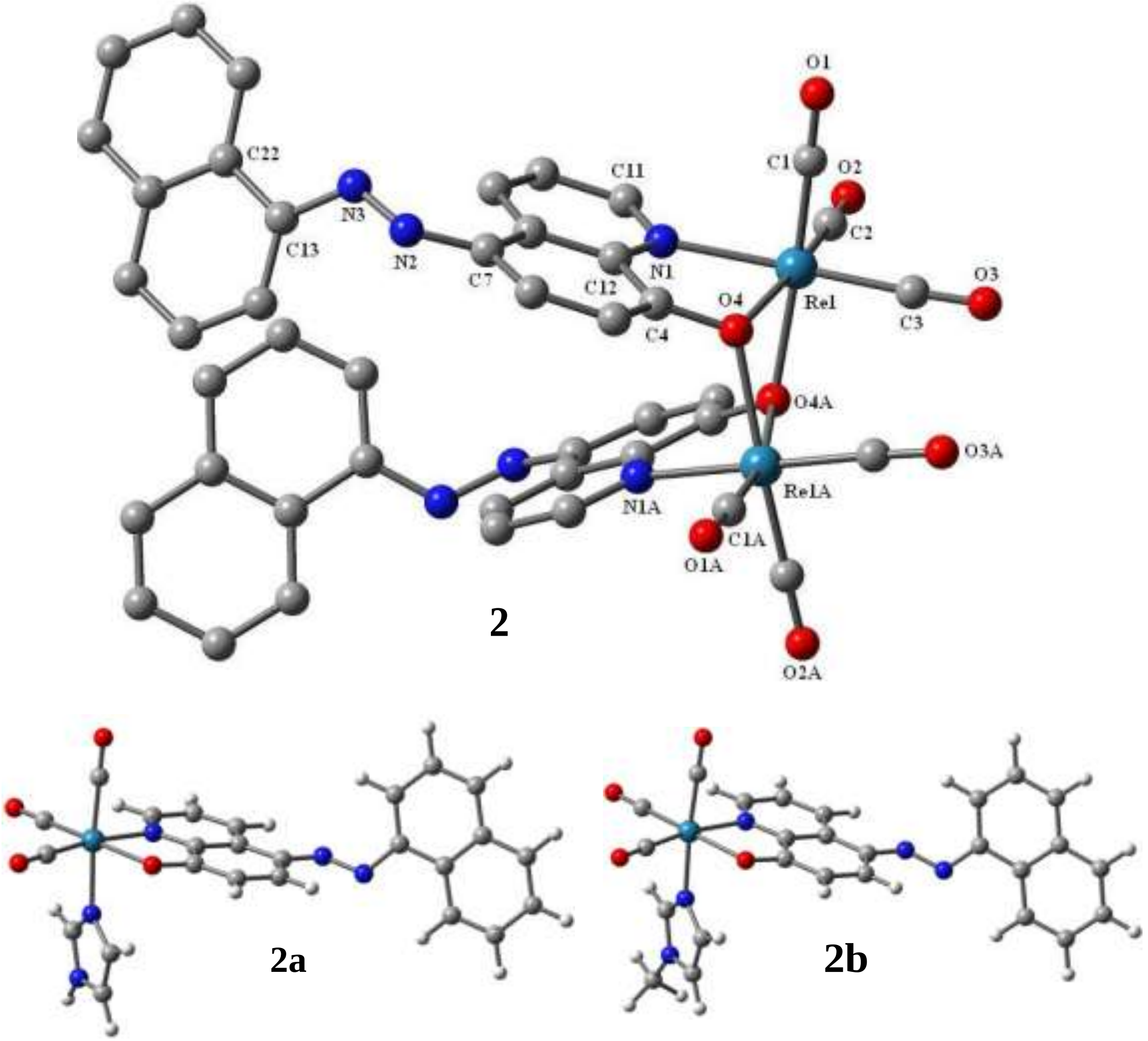

2

2a

2b

Fig. S4 Optimized molecular structures of [$Re_2(CO)_6(hq^2)_2$], **2**; [$Re(CO)_3(hq^2)(Im)$], **2a** and [$Re(CO)_3(hq^2)$(N-MeIm)], **2b** at T_1 state. (Re: Cyan, N: Blue, O: Red, C: Grey, H: White. All hydrogen atoms of **2** are omitted for clarity).

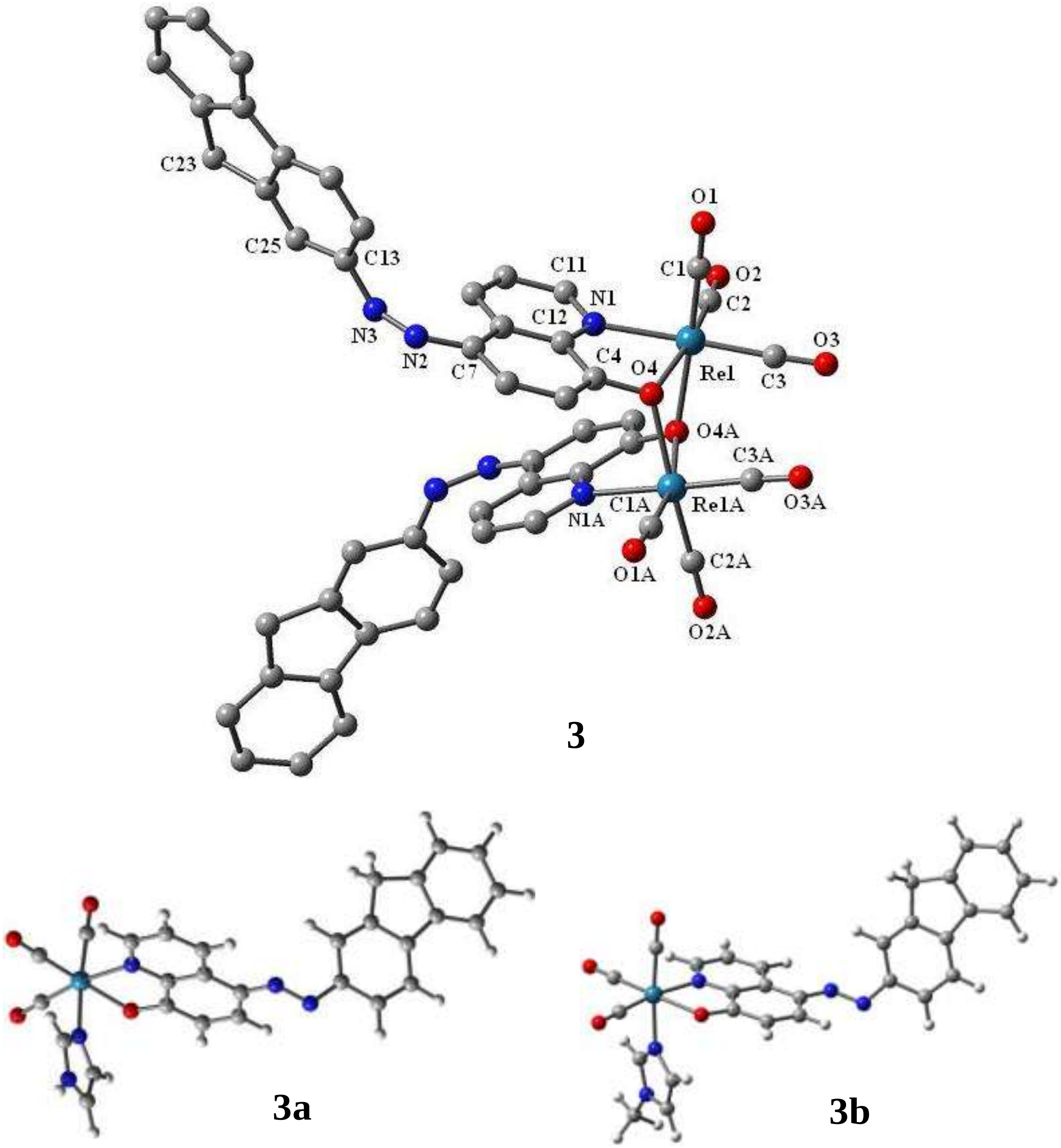

3

3a

3b

Fig. S5 Optimized molecular structures of $[Re_2(CO)_6(hq^3)_2]$, **3**; $[Re(CO)_3(hq^3)(Im)]$, **3a** and $[Re(CO)_3(hq^3)(N\text{-}MeIm)]$, **3b** at T_1 state. (Re: Cyan, N: Blue, O: Red, C: Grey, H: White. All hydrogen atoms of **3** are omitted for clarity).

Table S3 Frontier molecular orbital composition (%) in the ground state for [Re$_2$(CO)$_6$(hq^1)$_2$], **1**

Orbital	Energy (eV)	Contribution (%)					Main bond type
		Re	CO	Ligand (hq^1)			
				Quinoline	N=N	Aromatic system	
L+5	−1.585	24	68	7	1	1	p(Re)+π^*(CO)+π^*(hq^1)
L+4	−1.713	26	42	22	6	4	p(Re)+π^*(CO)+π^*(hq^1)
L+3	−1.961	3	7	59	20	12	π^*(CO)+π^*(hq^1)
L+2	−1.983	11	17	45	16	10	p(Re)+π^*(CO)+π^*(hq1)
L+1	−2.912	2	3	54	29	13	π^*(hq^1)
L	−2.925	1	1	57	28	13	π^*(hq^1)
H	−6.048	14	10	51	7	17	d(Re)+π(CO)+π(hq1)
H−1	−6.174	3	2	58	10	27	π(hq^1)
H−2	−6.289	0	0	11	79	9	π(hq^1)
H−3	−6.291	0	0	11	79	9	π(hq^1)
H−4	−6.630	63	29	7	1	1	d(Re)+π(CO)+π(hq^1)
H−5	−6.677	58	29	12	0	0	d(Re)+π(CO)+ π(hq^1)

Table S4 Frontier molecular orbital composition (%) in the ground state for [Re(CO)$_3$(hq^1)(N-MeIm)], **1b**

Orbital	Energy (eV)	Contribution (%)						Main bond type
		Re	CO	Ligand (hq^1)			Imi	
				Quinoline	N=N	Aromatic system		
L+5	−0.629	2	66	3	0	1	29	π^*(CO)+ π^*(Imi)
L+4	−1.097	1	1	95	0	0	2	π^*(hq^1)
L+3	−1.154	14	71	7	0	0	7	p(Re)+π^*(CO)+π^*(hq^1)+π^*(Imi)
L+2	−1.395	24	71	5	0	0	1	p(Re)+π^*(CO)+π^*(hq^1)
L+1	−2.072	1	4	70	16	9	0	π^*(CO)+π^*(hq^1)
L	−2.814	1	2	47	34	16	0	π^*(hq^1)
H	−5.677	7	5	64	9	14	0	d(Re)+π(CO)+π(hq^1)
H−1	−6.443	0	0	6	86	7	0	π(hq^1)
H−2	−6.580	57	28	6	0	0	9	d(Re)+π(CO)+π(hq^1)+π(Imi)
H−3	−6.687	51	25	11	2	7	3	d(Re)+π(CO)+π(hq^1)
H−4	−6.759	56	28	8	2	5	2	d(Re)+π(CO)+π(hq^1)
H−5	−7.232	2	1	2	1	6	90	π(hq^1)+π(Imi)

Table S5 Frontier molecular orbital composition (%) in the ground state for $[Re_2(CO)_6(hq^2)_2]$, **2**

Orbital	Energy (eV)	Contribution (%)					Main bond type
		Re	CO	Ligand (hq^2)			
				Quinoline	N=N	Aromatic system	
L+5	−1.592	24	68	7	0	1	p(Re)+π^*(CO)+π^*(hq^2)
L+4	−1.753	29	46	17	2	6	p(Re)+π^*(CO)+π^*(hq^2)
L+3	−2.045	3	6	59	14	18	π^*(CO)+π^*(hq^2)
L+2	−2.050	8	13	50	13	16	p(Re)+π^*(CO)+π^*(hq^2)
L+1	−2.959	2	2	48	29	18	π^*(hq^2)
L	−2.970	1	1	52	29	18	π^*(hq^2)
H	−5.789	4	3	31	11	51	d(Re)+π(hq^2)
H−1	−5.828	1	0	28	12	59	π(hq^2)
H−2	−6.304	0	0	10	71	19	π(hq^2)
H−3	−6.305	0	0	10	71	18	π(hq^2)
H−4	−6.410	28	17	23	5	28	d(Re)+π(CO)+ π(hq^2)
H−5	−6.595	53	24	13	2	8	d(Re)+π(CO)+ π(hq^2)

Table S6 Frontier molecular orbital composition (%) in the ground state for $[Re(CO)_3(hq^2)(Im)]$, **2a**

Orbital	Energy (eV)	Contribution (%)						Main bond type
		Re	CO	Ligand (hq^2)			Imi	
				Quinoline	N=N	Aromatic system		
L+5	−1.059	0	1	60	4	31	3	π^*(hq^2)
L+4	−1.151	5	21	37	5	31	1	p(Re)+π^*(CO)+π^*(hq^2)
L+3	−1.180	9	53	13	2	17	5	p(Re)+π^*(CO)+π^*(hq^2)+π^*(Imi)
L+2	−1.405	24	73	4	0	0	0	p(Re)+π^*(CO)+π^*(hq^2)
L+1	−2.131	1	4	72	10	13	0	π^*(CO)+π^*(hq^2)
L	−2.889	1	1	42	33	23	0	π^*(hq^2)
H	−5.568	5	4	53	8	30	0	d(Re)+π(CO)+π(hq^2)
H−1	−6.384	0	0	7	85	7	0	π(hq^2)
H−2	−6.402	16	9	14	5	55	1	d(Re)+π(CO)+π(hq^2)
H−3	−6.606	58	29	7	0	0	6	d(Re)+π(CO)+π(hq^2)+π(Imi)
H−4	−6.740	60	29	8	0	1	1	d(Re)+π(CO)+π(hq^2)
H−5	−6.911	38	17	19	3	16	7	d(Re)+π(CO)+π(hq^2)+π(Imi)

Table S7 Frontier molecular orbital composition (%) in the ground state for $[Re(CO)_3(hq^2)(N\text{-}MeIm)]$, **2b**

Orbital	Energy (eV)	Contribution (%)						Main bond type
		Re	CO	Ligand (hq^2)			Imi	
				Quinoline	N=N	Aromatic system		
L+5	−1.055	1	1	62	4	30	3	$\pi^*(hq^2)$
L+4	−1.142	8	38	28	4	20	2	$p(Re)+\pi^*(CO)+\pi^*(hq^2)$
L+3	−1.169	6	34	21	4	29	5	$p(Re)+\pi^*(CO)+\pi^*(hq^2)+\pi^*(Imi)$
L+2	−1.394	24	72	4	0	0	0	$p(Re)+\pi^*(CO)+\pi^*(hq^2)$
L+1	−2.126	1	4	72	10	13	0	$\pi^*(CO)+\pi^*(hq^2)$
L	−2.883	1	1	42	34	23	0	$\pi^*(hq^2)$
H	−5.559	5	3	53	8	30	0	$d(Re)+\pi(hq^2)$
H−1	−6.381	0	0	7	84	8	0	$\pi(hq^2)$
H−2	−6.391	17	9	13	6	53	2	$d(Re)+\pi(CO)+\pi(hq^2)$
H−3	−6.589	58	28	7	0	1	7	$d(Re)+\pi(CO)+\pi(hq^2)+\pi(Imi)$
H−4	−6.727	59	29	8	0	2	1	$d(Re)+\pi(CO)+\pi(hq^2)$
H−5	−6.882	36	16	19	3	17	9	$d(Re)+\pi(CO)+\pi(hq^2)+\pi(Imi)$

Table S8 Frontier molecular orbital composition (%) in the ground state for $[Re_2(CO)_6(hq^3)_2]$, **3**

Orbital	Energy (eV)	Contribution (%)					Main bond type
		Re	CO	Ligand (hq^3)			
				Quinoline	N=N	Aromatic system	
L+5	−1.575	24	67	7	1	1	$p(Re)+\pi^*(CO)+\pi^*(hq^3)$
L+4	−1.716	25	41	22	5	7	$p(Re)+\pi^*(CO)+\pi^*(hq^3)$
L+3	−1.975	3	7	57	16	16	$\pi^*(CO)+\pi^*(hq^3)$
L+2	−1.991	12	18	44	13	13	$p(Re)+\pi^*(CO)+\pi^*(hq^3)$
L+1	−2.896	2	2	51	28	17	$\pi^*(hq^3)$
L	−2.913	1	1	54	28	16	$\pi^*(hq^3)$
H	−5.783	4	3	32	7	54	$d(Re)+\pi(hq^3)$
H−1	−5.824	1	0	30	7	62	$\pi(hq^3)$
H−2	−6.239	0	0	11	79	9	$\pi(hq^3)$
H−3	−6.241	0	0	11	79	9	$\pi(hq^3)$
H−4	−6.406	27	17	22	4	31	$d(Re)+\pi(CO)+ \pi(hq^3)$
H−5	−6.582	53	24	12	2	9	$d(Re)+\pi(CO)+ \pi(hq^3)$

Table S9 Frontier molecular orbital composition (%) in the ground state for $[\mathrm{Re(CO)_3(hq^3)(Im)}]$, **3a**

Orbital	Energy (eV)	Contribution (%)						Main bond type
		Re	CO	Ligand ($\mathrm{hq^3}$)			Imi	
				Quinoline	N=N	Aromatic system		
L+5	−0.851	0	1	9	7	82	1	$\pi^*(\mathrm{hq}^3)$
L+4	−1.091	1	1	94	1	2	2	$\pi^*(\mathrm{hq}^3)$
L+3	−1.164	13	73	7	0	0	6	$\mathrm{p(Re)}+\pi^*(\mathrm{CO})+\pi^*(\mathrm{hq}^3)+\pi^*(\mathrm{Imi})$
L+2	−1.398	23	73	4	0	0	0	$\mathrm{p(Re)}+\pi^*(\mathrm{CO})+\pi^*(\mathrm{hq}^3)$
L+1	−2.093	1	4	70	12	12	0	$\pi^*(\mathrm{CO})+\pi^*(\mathrm{hq}^3)$
L	−2.821	1	2	44	32	21	0	$\pi^*(\mathrm{hq}^3)$
H	−5.545	5	4	55	8	28	0	$\mathrm{d(Re)}+\pi(\mathrm{CO})+\pi(\mathrm{hq}^3)$
H−1	−6.408	0	0	6	86	8	0	$\pi(\mathrm{hq3})$
H−2	−6.420	18	10	13	6	53	1	$\mathrm{d(Re)}+\pi(\mathrm{CO})+\pi(\mathrm{hq}^3)$
H−3	−6.599	58	29	7	0	0	6	$\mathrm{d(Re)}+\pi(\mathrm{CO})+\pi(\mathrm{hq}^3)+\pi(\mathrm{Imi})$
H−4	−6.730	59	29	8	0	2	1	$\mathrm{d(Re)}+\pi(\mathrm{CO})+\pi(\mathrm{hq}^3)$
H−5	−6.910	35	16	19	3	20	7	$\mathrm{d(Re)}+\pi(\mathrm{CO})+\pi(\mathrm{hq}^3)+\pi(\mathrm{Imi})$

Table S10 Frontier molecular orbital composition (%) in the ground state for $[\mathrm{Re(CO)_3(hq^3)(N\text{-}MeIm)}]$, **3b**

Orbital	Energy (eV)	Contribution (%)						Main bond type
		Re	CO	Ligand ($\mathrm{hq^3}$)			Imi	
				Quinoline	N=N	Aromatic system		
L+5	−0.849	0	1	10	7	82	1	$\pi^*(\mathrm{hq}^3)$
L+4	−1.085	1	1	94	1	2	2	$\pi^*(\mathrm{hq}^3)$
L+3	−1.145	14	71	7	0	0	8	$\mathrm{p(Re)}+\pi^*(\mathrm{CO})+\pi^*(\mathrm{hq}^3)+\pi^*(\mathrm{Imi})$
L+2	−1.384	23	72	4	0	0	1	$\mathrm{p(Re)}+\pi^*(\mathrm{CO})+\pi^*(\mathrm{hq}^3)$
L+1	−2.086	1	4	70	12	12	0	$\pi^*(\mathrm{hq}^3)$
L	−2.815	1	2	44	33	21	0	$\pi^*(\mathrm{hq}^3)$
H	−5.538	5	4	55	8	28	0	$\mathrm{d(Re)}+\pi(\mathrm{CO})+\pi(\mathrm{hq}^3)$
H−1	−6.402	1	0	6	85	8	0	$\pi(\mathrm{hq}^3)$
H−2	−6.411	19	10	12	7	51	2	$\mathrm{d(Re)}+\pi(\mathrm{CO})+\pi(\mathrm{hq}^3)$
H−3	−6.569	57	28	7	0	1	7	$\mathrm{d(Re)}+\pi(\mathrm{CO})+\pi(\mathrm{hq}^3)+\pi(\mathrm{Imi})$
H−4	−6.715	59	29	8	0	2	1	$\mathrm{d(Re)}+\pi(\mathrm{CO})+\pi(\mathrm{hq}^3)$
H−5	−6.890	34	16	19	3	20	9	$\mathrm{d(Re)}+\pi(\mathrm{CO})+\pi(\mathrm{hq}^3)+\pi(\mathrm{Imi})$

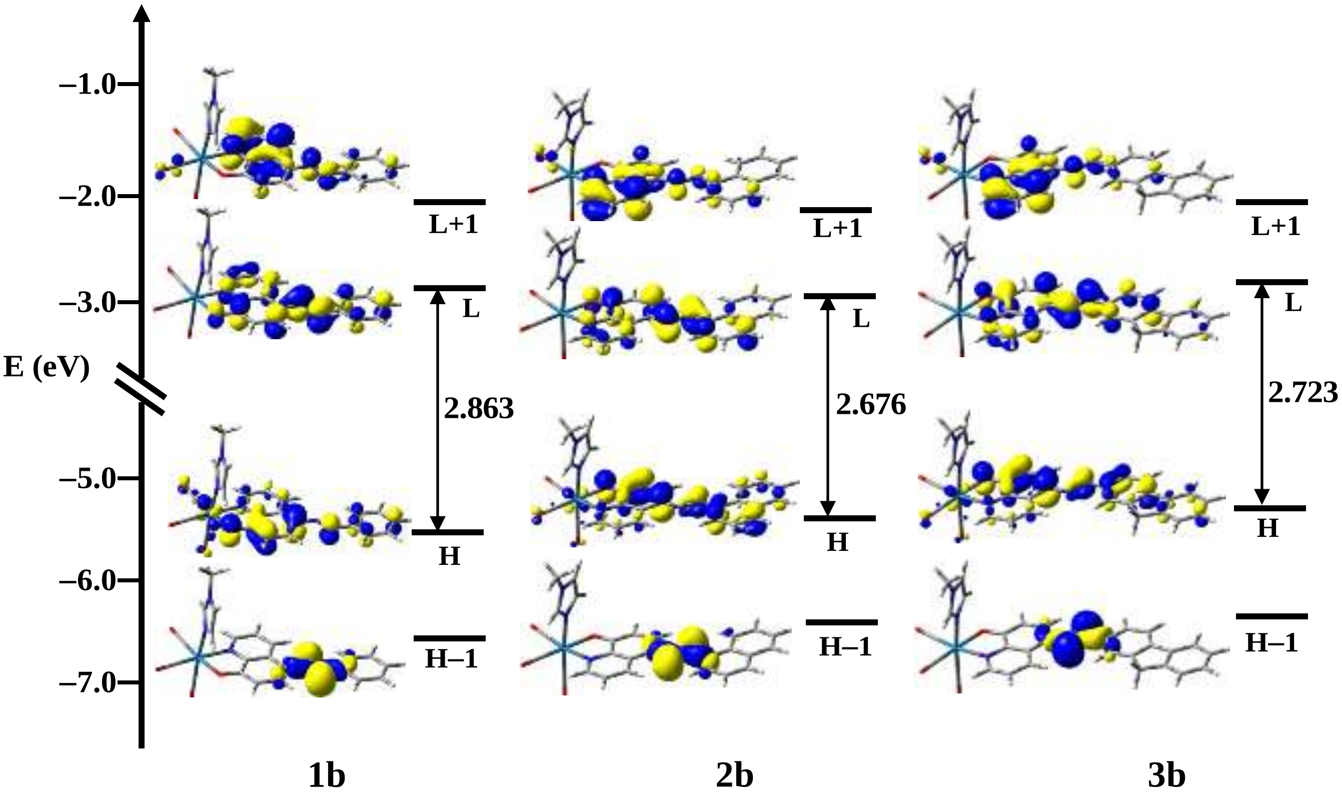

Fig. S6 Partial molecular orbital diagram with some isodensity frontier molecular orbital mainly involved in the electronic transitions for complexes [Re(CO)$_3$(hq^1)(N-MeIm)], **1b**; [Re(CO)$_3$(hq^2)(N-MeIm)], **2b** and [Re(CO)$_3$(hq^3)(N-MeIm)], **3b**.

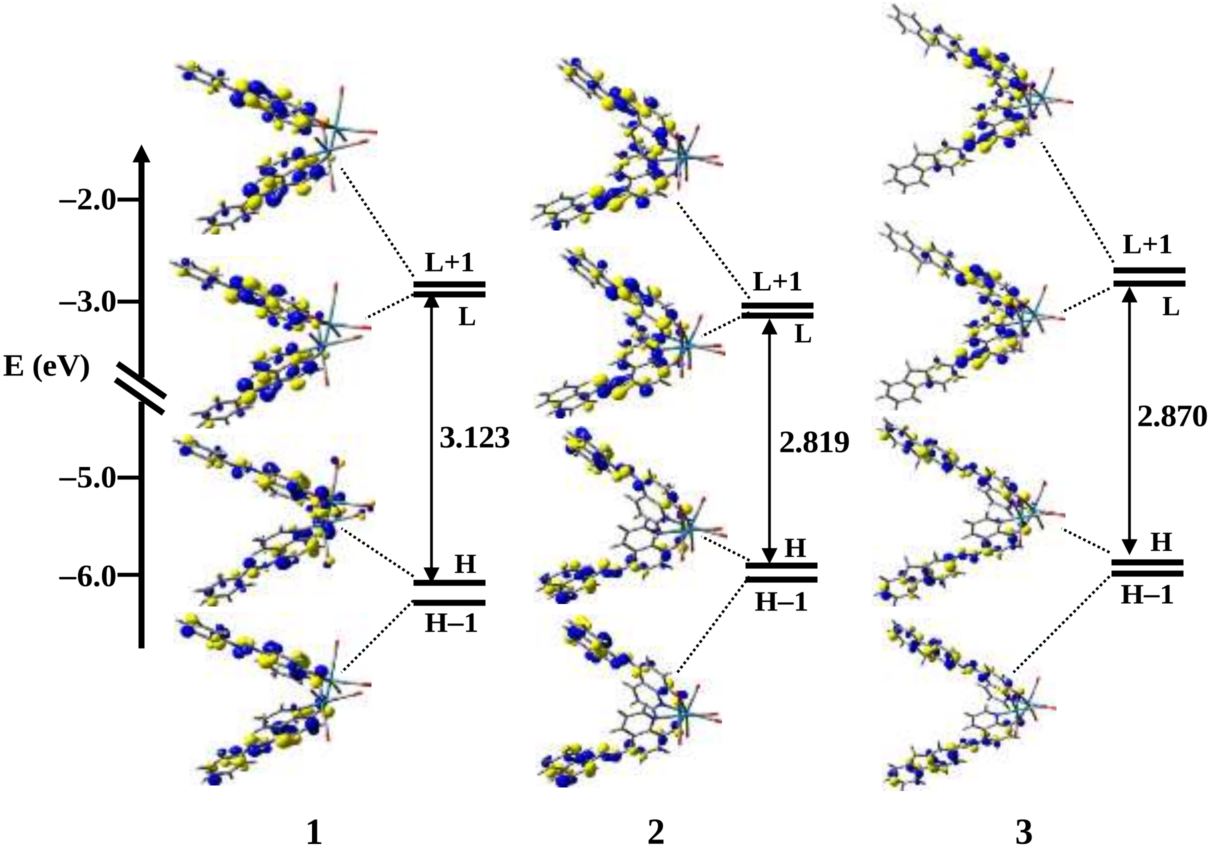

Fig. S7 Partial molecular orbital diagram with some isodensity frontier molecular orbital mainly involved in the electronic transitions for complexes $[Re_2(CO)_6(hq^1)_2]$, **1**; $[Re_2(CO)_6(hq^2)_2]$, **2** and $[Re_2(CO)_6(hq^3)_2]$, **3**.

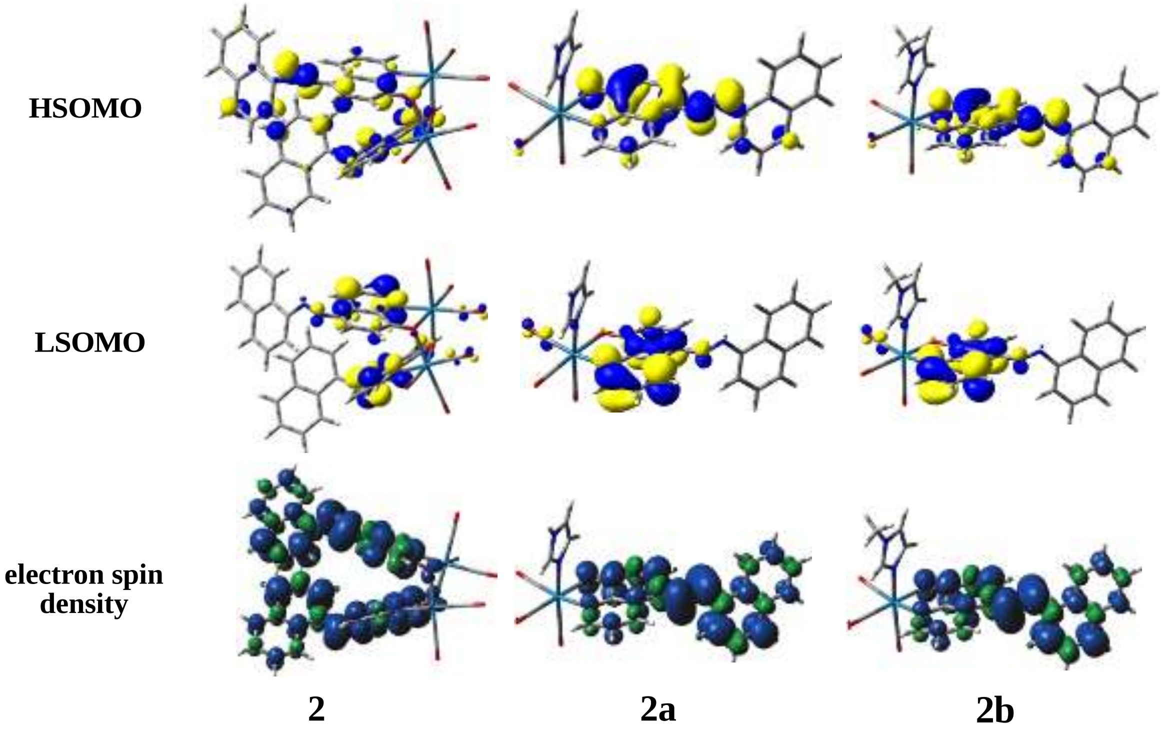

Fig. S8 Isodensity surface plots of the highest and lowest singly occupied molecular orbitals, HSOMO and LSOMO, respectively, along with the corresponding electron spin density, for the complexes [$Re_2(CO)_6(hq^2)_2$], **2**; [$Re(CO)_3(hq^2)(Im)$], **2a** and [$Re(CO)_3(hq^2)$(N-MeIm)], **2b** at their T_1 state geometry. Blue and green colors show regions of positive and negative difference between the alpha and beta electron densities, respectively.

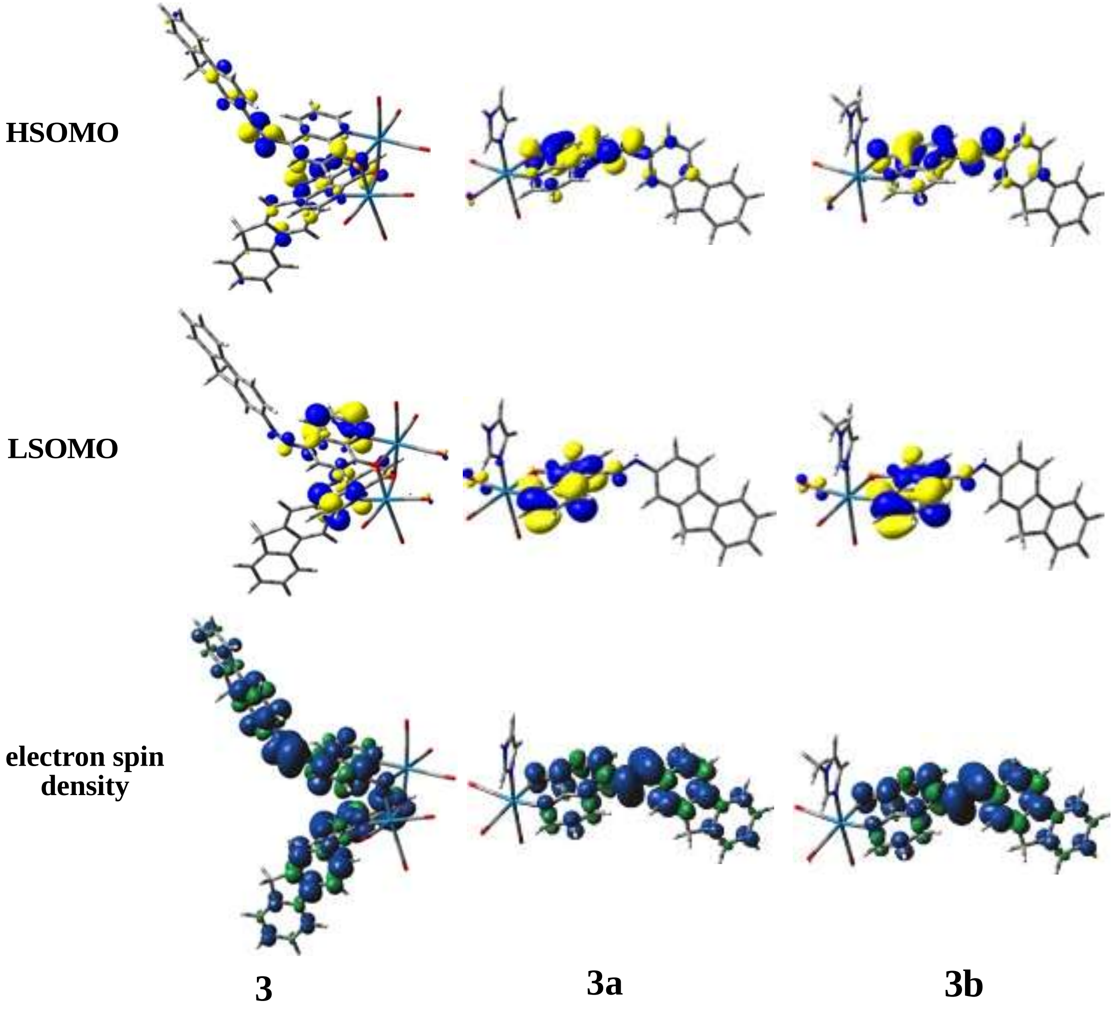

Figure S9. Isodensity surface plots of the highest and lowest singly occupied molecular orbitals, HSOMO and LSOMO, respectively, along with the corresponding electron spin density, for the complexes [$Re_2(CO)_6(hq^3)_2$], **3**; [$Re(CO)_3(hq^3)(Im)$], **3a** and [$Re(CO)_3(hq^3)$(N-MeIm)], **3b** at their T_1 state geometry. Blue and green colors show regions of positive and negative difference between the alpha and beta electron densities, respectively.

Table S11 The occupancies and composition of the calculated natural bond orbitals (NBOs) between the rhenium and carbonyl ligand for $[\mathrm{Re_2(CO)_6(hq^2)_2}]$, **2;** $[\mathrm{Re(CO)_3(hq^2)(Im)}]$, **2a** and $[\mathrm{Re(CO)_3(hq^2)(N\text{-}MeIm)}]$, **2b**

		2		
BD	Occupancy	Composition of NBO	BD[a]	Occupancy
Re–CO (1)	1.9705	$0.6124(\mathrm{spd})_{\mathrm{Re}} + 0.7905(\mathrm{sp})_{\mathrm{C}}$	$0.7905(\mathrm{spd})_{\mathrm{Re}} - 0.6124(\mathrm{sp})_{\mathrm{C}}$	0.1758
Re–CO (2)	1.9661	$0.6001(\mathrm{spd})_{\mathrm{Re}} + 0.7999(\mathrm{sp})_{\mathrm{C}}$	$0.7999(\mathrm{spd})_{\mathrm{Re}} - 0.6001(\mathrm{sp})_{\mathrm{C}}$	0.1996
Re–CO (3)	1.9727	$0.6177(\mathrm{spd})_{\mathrm{Re}} + 0.7864(\mathrm{sp})_{\mathrm{C}}$	$0.7864(\mathrm{spd})_{\mathrm{Re}} - 0.6177(\mathrm{sp})_{\mathrm{C}}$	0.2154
Re–$\mathrm{N_{pyridyl}}$	1.6010	$0.9069(\mathrm{spd})_{\mathrm{Re}} + 0.4214(\mathrm{sp})_{\mathrm{N}}$	$0.4214(\mathrm{spd})_{\mathrm{Re}} - 0.9069(\mathrm{sp})_{\mathrm{N}}$	1.2336
		2a		
BD	Occupancy	Composition of NBO	BD[a]	Occupancy
Re–CO (1)	1.9705	$0.6092(\mathrm{spd})_{\mathrm{Re}} + 0.7930(\mathrm{sp})_{\mathrm{C}}$	$0.7930(\mathrm{spd})_{\mathrm{Re}} - 0.6092(\mathrm{sp})_{\mathrm{C}}$	0.2016
Re–CO (2)	1.9717	$0.6128(\mathrm{spd})_{\mathrm{Re}} + 0.7902(\mathrm{sp})_{\mathrm{C}}$	$0.7902(\mathrm{spd})_{\mathrm{Re}} - 0.6128(\mathrm{sp})_{\mathrm{C}}$	0.2122
Re–CO (3)	1.9727	$0.6175(\mathrm{spd})_{\mathrm{Re}} + 0.7866(\mathrm{sp})_{\mathrm{C}}$	$0.7866(\mathrm{spd})_{\mathrm{Re}} - 0.6175(\mathrm{sp})_{\mathrm{C}}$	0.2064
		2b		
BD	Occupancy	Composition of NBO	BD[a]	Occupancy
Re–CO (1)	1.9704	$0.6090(\mathrm{spd})_{\mathrm{Re}} + 0.7932(\mathrm{sp})_{\mathrm{C}}$	$0.7932(\mathrm{spd})_{\mathrm{Re}} - 0.6090(\mathrm{sp})_{\mathrm{C}}$	0.2023
Re–CO (2)	1.9717	$0.6129(\mathrm{spd})_{\mathrm{Re}} + 0.7901(\mathrm{sp})_{\mathrm{C}}$	$0.7901(\mathrm{spd})_{\mathrm{Re}} - 0.6129(\mathrm{sp})_{\mathrm{C}}$	0.2123
Re–CO (3)	1.9728	$0.6177(\mathrm{spd})_{\mathrm{Re}} + 0.7864(\mathrm{sp})_{\mathrm{C}}$	$0.7864(\mathrm{spd})_{\mathrm{Re}} - 0.6177(\mathrm{sp})_{\mathrm{C}}$	0.2066

BD denotes 2-center bond. [a] Denotes antibond NBO.

Table S12 The occupancies and composition of the calculated natural bond orbitals (NBOs) between the rhenium and carbonyl ligand for [Re$_2$(CO)$_6$(hq^3)$_2$], **3;** [Re(CO)$_3$(hq^3)(Im)], **3a** and [Re(CO)$_3$(hq^3)(N-MeIm)], **3b**

		3		
BD	Occupancy	Composition of NBO	BD[a]	Occupancy
Re–CO (1)	1.9705	0.6125(spd)$_{Re}$ + 0.7904(sp)$_C$	0.7904(spd)$_{Re}$ – 0.6125(sp)$_C$	0.1759
Re–CO (2)	1.9662	0.6002(spd)$_{Re}$ + 0.7999(sp)$_C$	0.7999(spd)$_{Re}$ – 0.6002(sp)$_C$	0.2001
Re–CO (3)	1.9728	0.6176(spd)$_{Re}$ + 0.7865(sp)$_C$	0.7865(spd)$_{Re}$ – 0.6176(sp)$_C$	0.2155
Re–N$_{pyridyl}$	1.6004	0.9064(spd)$_{Re}$ + 0.4225(sp)$_N$	0.4225(spd)$_{Re}$ – 0.9064(sp)$_N$	1.2344
		3a		
BD	Occupancy	Composition of NBO	BD[a]	Occupancy
Re–CO (1)	1.9705	0.6093(spd)$_{Re}$ + 0.7930(sp)$_C$	0.7930(spd)$_{Re}$ – 0.6093(sp)$_C$	0.2019
Re–CO (2)	1.9717	0.6127(spd)$_{Re}$ + 0.7903(sp)$_C$	0.7903(spd)$_{Re}$ – 0.6127(sp)$_C$	0.2119
Re–CO (3)	1.9727	0.6175(spd)$_{Re}$ + 0.7866(sp)$_C$	0.7866(spd)$_{Re}$ – 0.6175(sp)$_C$	0.2067
		3b		
BD	Occupancy	Composition of NBO	BD[a]	Occupancy
Re–CO (1)	1.9704	0.6091(spd)$_{Re}$ + 0.7931(sp)$_C$	0.7931(spd)$_{Re}$ – 0.6091(sp)$_C$	0.2024
Re–CO (2)	1.9717	0.6127(spd)$_{Re}$ + 0.7903(sp)$_C$	0.7903(spd)$_{Re}$ – 0.6127(sp)$_C$	0.2118
Re–CO (3)	1.9728	0.6177(spd)$_{Re}$ + 0.7864(sp)$_C$	0.7864(spd)$_{Re}$ – 0.6177(sp)$_C$	0.2068

BD denotes 2-center bond. [a] Denotes antibond NBO.

Table S13 Main calculated optical transition for the complex [Re(CO)$_3$(hq^1)(N-MeIm)], **1b** with composition in terms of molecular orbital contribution of the transition, vertical excitation energies, and oscillator strength in acetonitrile

Electronic Transitions	Composition	Excitation energy	Oscillator strength (f)	CI	Assign	λ_{exp} (nm)
$S_0 \rightarrow S_2$	$H \rightarrow L$	2.5884 eV	0.777	0.681	^{1}MLCT / ^{1}ILCT	475
	$H \rightarrow L + 1$	(479 nm)		0.167	^{1}MLCT / ^{1}ILCT	
$S_0 \rightarrow S_3$	$H \rightarrow L + 1$	3.0684 eV	0.301	0.138	^{1}MLCT / ^{1}ILCT	402
	$H \rightarrow L$	(404 nm)		–0.167	^{1}MLCT / ^{1}ILCT	
	$H - 2 \rightarrow L$			0.668	^{1}MLCT / ^{1}ILCT	
$S_0 \rightarrow S_6$	$H - 4 \rightarrow L$	3.445 eV	0.061	0.577	^{1}MLCT / ^{1}ILCT	356
	$H - 4 \rightarrow L + 1$	(359 nm)		0.109	^{1}MLCT / ^{1}ILCT	
	$H - 3 \rightarrow L$			–0.341	^{1}MLCT / ^{1}ILCT	
	$H - 2 \rightarrow L$			–0.125	^{1}MLCT / ^{1}ILCT	
$S_0 \rightarrow S_{20}$	$H - 8 \rightarrow L$	4.434 eV	0.083	0.478	^{1}ILCT	275
	$H - 4 \rightarrow L + 4$	(279 nm)		0.197	^{1}MLCT / ^{1}ILCT	
	$H - 3 \rightarrow L + 2$			0.196	^{1}MLCT / ^{1}ILCT	
	$H - 8 \rightarrow L + 3$			0.102	^{1}ILCT	
	$H - 2 \rightarrow L + 4$			0.195	^{1}MLCT / ^{1}ILCT	
	$H \rightarrow L + 3$			–0.248	^{1}MLCT / ^{1}ILCT	
	$H \rightarrow L + 5$			–0.146	^{1}MLCT / ^{1}ILCT	

Table S14 Main calculated optical transition for the complex [$Re_2(CO)_6(hq^2)_2$], **2** and [$Re(CO)_3(hq^2)(Im)$], **2a** with composition in terms of molecular orbital contribution of the transition, vertical excitation energies, and oscillator strength in acetonitrile

Complex	Electronic Transitions	Composition	Excitation energy	Oscillator strength (*f*)	CI	Assign	λ_{exp} (nm)
2	$S_0 \rightarrow S_2$	H – 3 → L + 1	2.1323 eV (581 nm)	0.0784	0.416	^{1}ILCT	572
		H – 2 → L			0.243	^{1}ILCT	
		H – 1 → L			0.231	^{1}ILCT	
		H → L + 2			0.421	^{1}MLCT / ^{1}ILCT	
	$S_0 \rightarrow S_3$	H – 3 → L	2.4524 eV (505 nm)	0.1261	–0.148	^{1}ILCT	532
		H – 2 → L + 1			–0.172	^{1}ILCT	
		H – 1 → L + 1			–0.162	^{1}ILCT	
		H → L + 1			0.639	^{1}MLCT / ^{1}ILCT	
	$S_0 \rightarrow S_{16}$	H – 3 → L	3.2062 eV (386 nm)	0.0764	0.221	^{1}ILCT	251
		H – 2 → L + 1			0.174	^{1}ILCT	
		H – 1 → L + 1			–0.158	^{1}ILCT	
		H → L			–0.337	^{1}MLCT / ^{1}ILCT	
		H – 6 → L			0.492	^{1}MLCT / ^{1}ILCT	
2a	$S_0 \rightarrow S_2$	H → L	2.3819 eV (520 nm)	0.9778	0.6972	^{1}MLCT / ^{1}ILCT	488
	$S_0 \rightarrow S_3$	H → L+1	2.8825 eV (430 nm)	0.1224	0.6937	^{1}MLCT / ^{1}ILCT	356
	$S_0 \rightarrow S_{22}$	H – 8 → L	4.3023 eV (288 nm)	0.0898	0.502	^{1}ILCT	277
		H – 5 → L + 2			0.183	^{1}MLCT / ^{1}ILCT	
		H – 3 → L + 4			0.100	^{1}MLCT / ^{1}ILCT	
		H – 2 → L + 3			–0.209	^{1}MLCT / ^{1}ILCT	
		H → L + 4			–0.153	^{1}MLCT / ^{1}ILCT	
		H → L + 5			–0.256	^{1}MLCT / ^{1}ILCT	

Table S15 Main calculated optical transition for the complex [Re(CO)$_3$(hq^2)(N-MeIm)], **2b** with composition in terms of molecular orbital contribution of the transition, vertical excitation energies, and oscillator strength in acetonitrile

Electronic Transitions	Composition	Excitation energy	Oscillator strength (f)	CI	Assign	λ_{exp} (nm)
$S_0 \rightarrow S_2$	H → L	2.418 eV (512 nm)	0.967	0.695	^{1}MLCT / ^{1}ILCT	488
$S_0 \rightarrow S_3$	H→ L	2.913 eV (425 nm)	0.167	0.105	^{1}MLCT / ^{1}ILCT	355
	H → L + 1			0.689	^{1}MLCT / ^{1}ILCT	
$S_0 \rightarrow S_{24}$	H – 6 → L	4.387 eV (282 nm)	0.0653	0.200	^{1}ILCT	276
	H – 6 → L + 1			–0.353	^{1}ILCT	
	H – 6 → L + 3			–0.114	^{1}ILCT	
	H – 6 → L + 5			–0.121	^{1}ILCT	
	H – 2→ L + 6			0.109	^{1}MLCT / ^{1}ILCT	
	H → L + 6			0.535	^{1}MLCT / ^{1}ILCT	

Table S16 Main calculated optical transition for the complex $[Re_2(CO)_6(hq^3)_2]$, **3** and $[Re(CO)_3(hq^3)(Im)]$**, 3a** with composition in terms of molecular orbital contribution of the transition, vertical excitation energies, and oscillator strength in acetonitrile

Complex	Electronic Transitions	Composition	Excitation energy	Oscillator strength (*f*)	CI	Assign	λ_{exp} (nm)
3	$S_0 \rightarrow S_2$	$H-3 \rightarrow L+1$	2.1933 eV (565 nm)	0.0004	–0.479	^{1}ILCT	597
		$H-3 \rightarrow L+3$			0.110	^{1}ILCT	
		$H-2 \rightarrow L$			0.489	^{1}ILCT	
		$H-2 \rightarrow L+2$			0.102	^{1}ILCT	
	$S_0 \rightarrow S_3$	$H-1 \rightarrow L+2$	2.4674 eV (502 nm)	0.4324	–0.179	^{1}ILCT	525
		$H \rightarrow L$			0.677	^{1}MLCT / ^{1}ILCT	
	$S_0 \rightarrow S_{13}$	$H-8 \rightarrow L+1$	3.1928 eV (388 nm)	0.0433	–0.101	^{1}MLCT / ^{1}ILCT	254
		$H-7 \rightarrow L$			–0.139	^{1}MLCT / ^{1}ILCT	
		$H-6 \rightarrow L$			0.665	^{1}MLCT / ^{1}ILCT	
3a	$S_0 \rightarrow S_2$	$H \rightarrow L$	2.450 eV (505 nm)	1.206	0.693	^{1}MLCT / ^{1}ILCT	490
		$H \rightarrow L+1$			0.109	^{1}MLCT / ^{1}ILCT	
	$S_0 \rightarrow S_5$	$H-4 \rightarrow L$	3.240 eV (382 nm)	0.045	0.259	^{1}MLCT / ^{1}ILCT	358
		$H-3 \rightarrow L$			–0.143	^{1}MLCT / ^{1}ILCT	
		$H-2 \rightarrow L$			0.618	^{1}MLCT / ^{1}ILCT	
	$S_0 \rightarrow S_{23}$	$H-9 \rightarrow L$	4.397 eV (281 nm)	0.048	–0.247	^{1}ILCT	277
		$H-7 \rightarrow L$			0.218	^{1}ILCT	
		$H-7 \rightarrow L+1$			0.109	^{1}ILCT	
		$H \rightarrow L+4$			0.129	^{1}MLCT / ^{1}ILCT	
		$H \rightarrow L+5$			–0.281	^{1}MLCT / ^{1}ILCT	
		$H \rightarrow L+6$			0.466	^{1}MLCT / ^{1}ILCT	
		$H \rightarrow L+7$			0.138	^{1}MLCT / ^{1}ILCT	
	$S_0 \rightarrow S_{33}$	$H-10 \rightarrow L$	4.762 eV (260 nm)	0.026	–0.292	^{1}ILCT	256
		$H-8 \rightarrow L+1$			0.603	^{1}MLCT / ^{1}ILCT	

Table S17 Main calculated optical transition for the complex [Re(CO)$_3$(hq^3)(N-MeIm)], **3b** with composition in terms of molecular orbital contribution of the transition, vertical excitation energies, and oscillator strength in acetonitrile

Electronic Transitions	Composition	Excitation energy	Oscillator strength (*f*)	CI	Assign	λ_{exp} (nm)
$S_0 \rightarrow S_2$	H → L	2.450 eV	1.212	0.695	^{1}MLCT / ^{1}ILCT	490
	H → L+1	(506 nm)		0.109	^{1}MLCT / ^{1}ILCT	
$S_0 \rightarrow S_5$	H – 4 → L	3.235 eV	0.059	0.234	^{1}MLCT / ^{1}ILCT	358
	H – 2 → L	(383 nm)		0.637	^{1}MLCT / ^{1}ILCT	
$S_0 \rightarrow S_{23}$	H – 9 → L	4.397 eV	0.063	–0.342	^{1}ILCT	277
	H – 8 → L	(281 nm)		0.199	^{1}ILCT	
	H → L + 3			0.152	^{1}MLCT / ^{1}ILCT	
	H → L + 5			–0.207	^{1}MLCT / ^{1}ILCT	
	H → L + 6			0.446	^{1}MLCT / ^{1}ILCT	
	H → L + 7			–0.135	^{1}MLCT / ^{1}ILCT	
$S_0 \rightarrow S_{36}$	H – 11 → L	4.779 eV	0.035	0.207	^{1}MLCT / ^{1}ILCT	256
	H – 10 → L + 3	(259 nm)		0.493	^{1}ILCT	
	H – 9 → L + 1			0.114	^{1}ILCT	
	H – 3 → L + 3			–0.269	^{1}MLCT / ^{1}ILCT	
	H – 2 → L + 3			–0.277	^{1}MLCT / ^{1}ILCT	

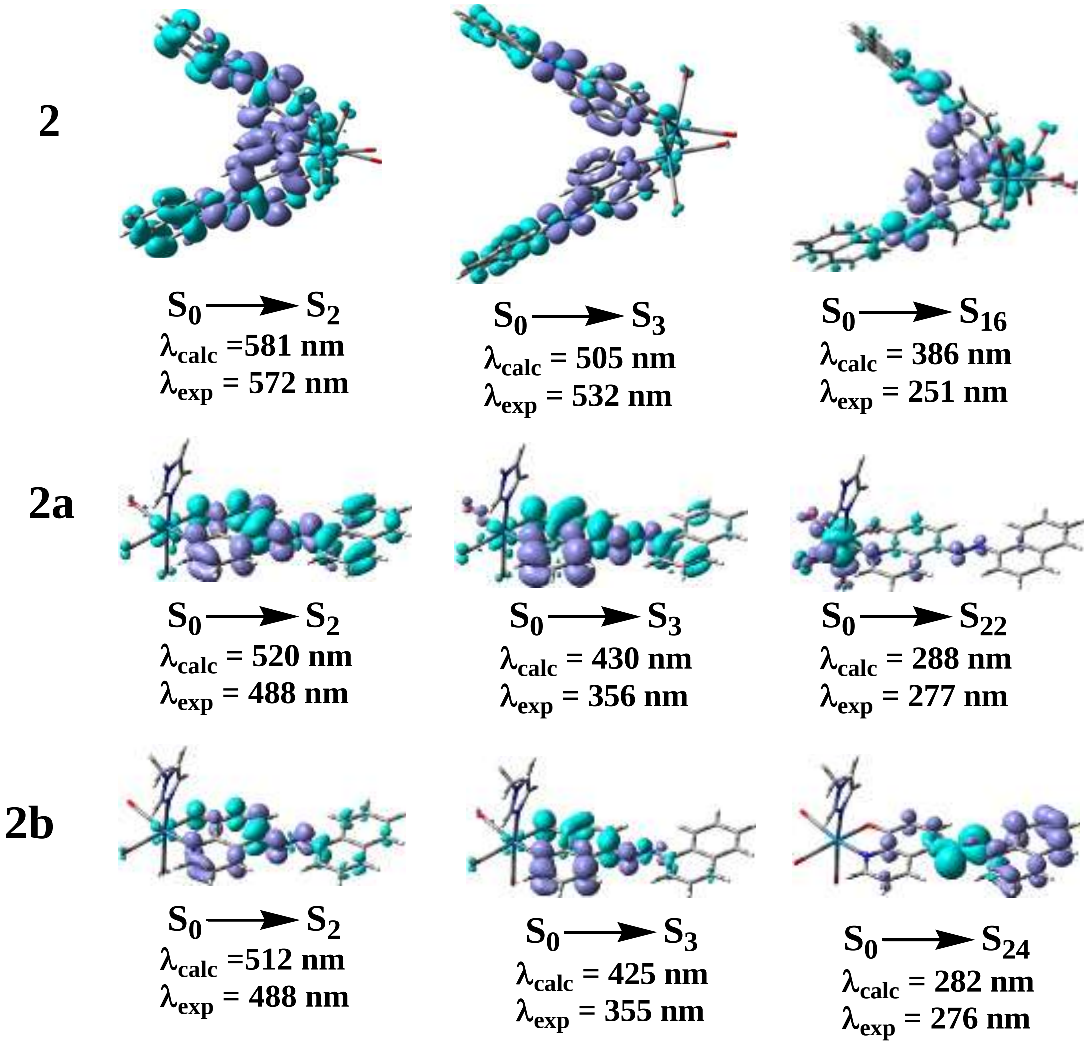

Fig. S10 Difference electron density upon excitation from the ground state (S_0) to allowed singlet states (40 singlet to singlet excitations) for complexes $[Re_2(CO)_6(hq^2)_2]$, **2**; $[Re(CO)_3(hq^2)(Im)]$, **2a** and $[Re(CO)_3(hq^2)(N\text{-}MeIm)]$, **2b** determined with TD-DFT (B3LYP/CPCM-Acetonitrile) calculations. Turquoise and purple colors show regions of decreasing and increasing electron density, respectively.

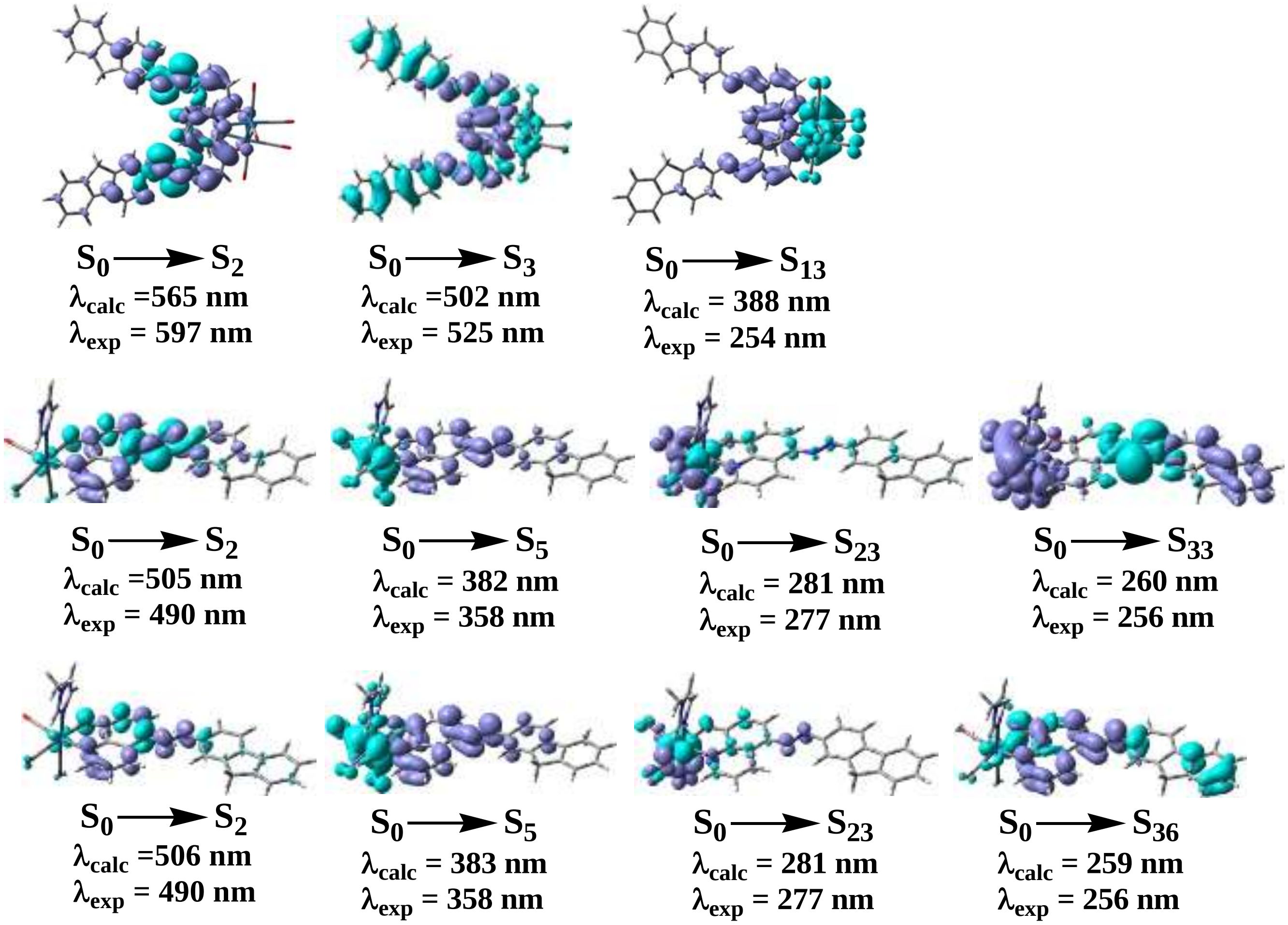

3

$S_0 \longrightarrow S_2$ λ_{calc} =565 nm λ_{exp} = 597 nm

$S_0 \longrightarrow S_3$ λ_{calc} =502 nm λ_{exp} = 525 nm

$S_0 \longrightarrow S_{13}$ λ_{calc} = 388 nm λ_{exp} = 254 nm

3a

$S_0 \longrightarrow S_2$ λ_{calc} =505 nm λ_{exp} = 490 nm

$S_0 \longrightarrow S_5$ λ_{calc} = 382 nm λ_{exp} = 358 nm

$S_0 \longrightarrow S_{23}$ λ_{calc} = 281 nm λ_{exp} = 277 nm

$S_0 \longrightarrow S_{33}$ λ_{calc} = 260 nm λ_{exp} = 256 nm

3b

$S_0 \longrightarrow S_2$ λ_{calc} =506 nm λ_{exp} = 490 nm

$S_0 \longrightarrow S_5$ λ_{calc} = 383 nm λ_{exp} = 358 nm

$S_0 \longrightarrow S_{23}$ λ_{calc} = 281 nm λ_{exp} = 277 nm

$S_0 \longrightarrow S_{36}$ λ_{calc} = 259 nm λ_{exp} = 256 nm

Fig. S11 Difference electron density upon excitation from the ground state (S_0) to allowed singlet states (40 singlet to singlet excitations) for complexes [$Re_2(CO)_6(hq^3)_2$], **3**; [$Re(CO)_3(hq^3)(Im)$], **3a** and [$Re(CO)_3(hq^3)$(N-MeIm)], **3b** determined with TD-DFT (B3LYP/CPCM-Acetonitrile) calculations. Turquoise and purple colors show regions of decreasing and increasing electron density, respectively.

^{1}MLCT / ^{1}ILCT		Hole	Electron
λ_{exp} = 550 nm	S$_3$ w = 0.97 2.641 ev (0.17) $t_{2g} - \pi \rightarrow \pi^*$	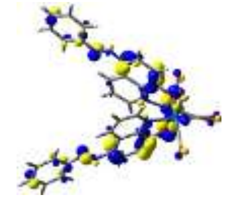	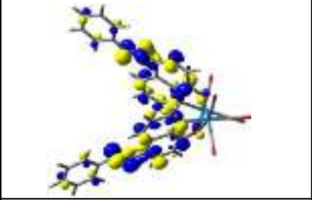
λ_{exp} = 253 nm	S$_{31}$ w = 0.28 3.377 ev (0.08) $t_{2g} - \pi \rightarrow \pi^*$	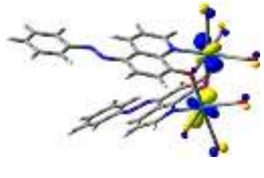	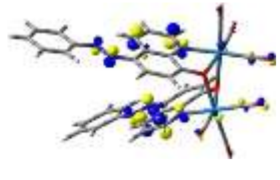

Fig. S12 Natural transition orbitals (NTOs) for the complexes [Re$_2$(CO)$_6$(hq^1)$_2$], **1** illustrating the nature of optically active singlet excited states in the absorption bands 550 and 253 nm. For each state, the respective number of the state, transition energy (eV), and the oscillator strength (in parentheses) are listed. Shown are only occupied (holes) and unoccupied (electrons) NTO pairs that contribute more than 25% to each excited state. All transitions are mixed ^{1}MLCT/^{1}ILCT character: charge is transferred from $t_{2g} - \pi$ hole orbital to the π^*orbital of the ligands.

^{1}MLCT / ^{1}ILCT			Hole	Electron
488 nm	**2a**	S_2 w = 0.97 2.382 ev (0.98) $t_{2g} - \pi \rightarrow \pi^*$	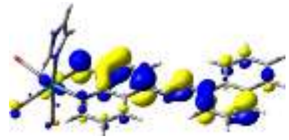	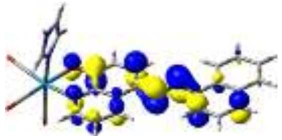
	2b	S_2 w = 0.96 2.418 ev (0.96) $t_{2g} - \pi \rightarrow \pi^*$	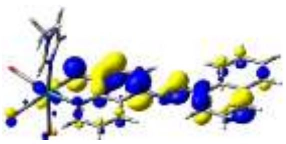	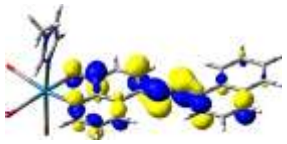
~ 355 nm	**2a**	S_3 w = 0.96 2.883 ev (0.12) $t_{2g} - \pi \rightarrow \pi^*$		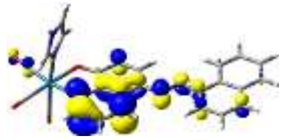
	2b	S_3 w = 0.95 2.913 ev (0.16) $t_{2g} - \pi \rightarrow \pi^*$	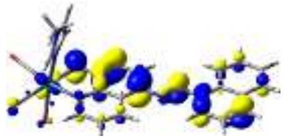	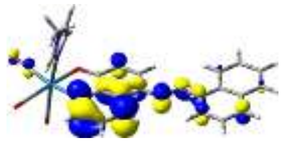
~ 277 nm	**2a**	S_{22} w = 0.50 4.302 ev (0.08) $t_{2g} - \pi \rightarrow \pi^*$	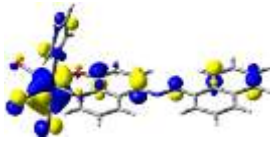	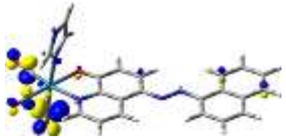
	2b	S_{24} w = 0.57 4.387 ev (0.07) $t_{2g} - \pi \rightarrow \pi^*$	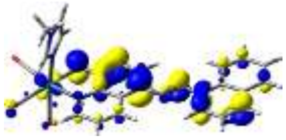	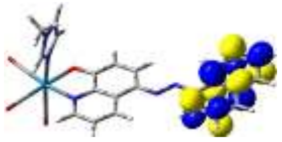

Fig. S13 Natural transition orbitals (NTOs) for the complexes [Re(CO)$_3$(hq^2)(Im)], **2a** and [Re(CO)$_3$(hq^2)(N-MeIm)], **2b** illustrating the nature of optically active singlet excited states in the absorption bands 488, ~ 355 and ~ 277 nm. For each state, the respective number of the state, transition energy (eV), and the oscillator strength (in parentheses) are listed. Shown are only occupied (holes) and unoccupied (electrons) NTO pairs that contribute more than 30% to each excited state. All transitions are mixed ^{1}MLCT/^{1}ILCT character: charge is transferred from $t_{2g} - \pi$ hole orbital to the π^*orbital of the ligands.

^{1}MLCT / ^{1}ILCT			Hole	Electron
~ 490 nm	**3a**	S_2 w = 0.96 2.450 ev (1.20) $t_{2g} - \pi \rightarrow \pi^*$	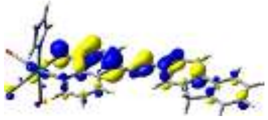	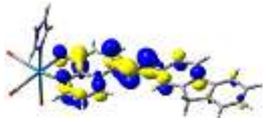
	3b	S_2 w = 0.96 2.450 ev (1.21) $t_{2g} - \pi \rightarrow \pi^*$	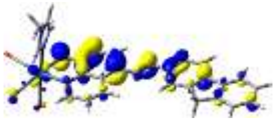	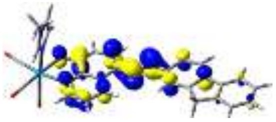
358 nm	**3a**	S_5 w = 0.76 3.240 ev (0.04) $t_{2g} - \pi \rightarrow \pi^*$	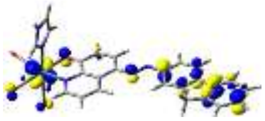	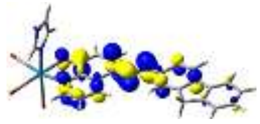
	3b	S_5 w = 0.81 3.235 ev (0.06) $t_{2g} - \pi \rightarrow \pi^*$	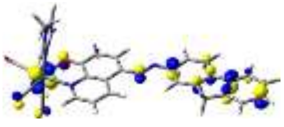	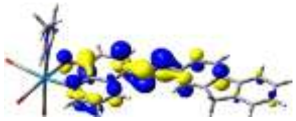
277 nm	**3a**	S_{23} w = 0.43 4.397 ev (0.05) $t_{2g} - \pi \rightarrow \pi^*$	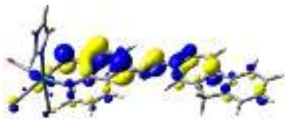	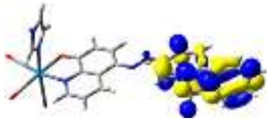
	3b	S_{23} w = 0.39 4.397 ev (0.06) $t_{2g} - \pi \rightarrow \pi^*$	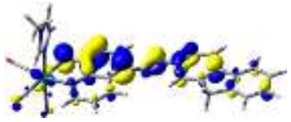	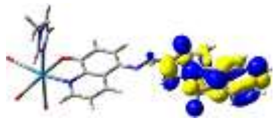
256 nm	**3a**	S_{33} w = 0.72 4.762 ev (0.03) $t_{2g} - \pi \rightarrow \pi^*$		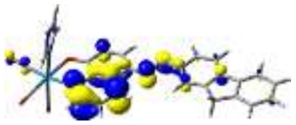
	3b	S_{36} w = 0.48 4.779 ev (0.04) $t_{2g} - \pi \rightarrow \pi^*$	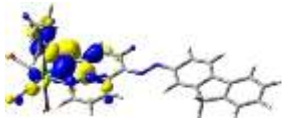	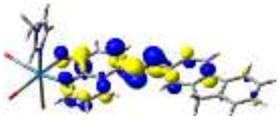

Fig. S14 Natural transition orbitals (NTOs) for the complexes [Re(CO)$_3$(hq^3)(Im)], **3a** and [Re(CO)$_3$(hq^3)(N-MeIm)], **3b** illustrating the nature of optically active singlet excited states in the absorption bands ~ 490, 358, 277 and 256 nm. For each state, the respective number of the state, transition energy (eV), and the oscillator strength (in parentheses) are listed. Shown are only occupied (holes) and unoccupied (electrons) NTO pairs that contribute more than 30% to each excited state. All transitions are mixed ^{1}MLCT/^{1}ILCT character: charge is transferred from $t_{2g} - \pi$ hole orbital to the π^*orbital of the ligands.

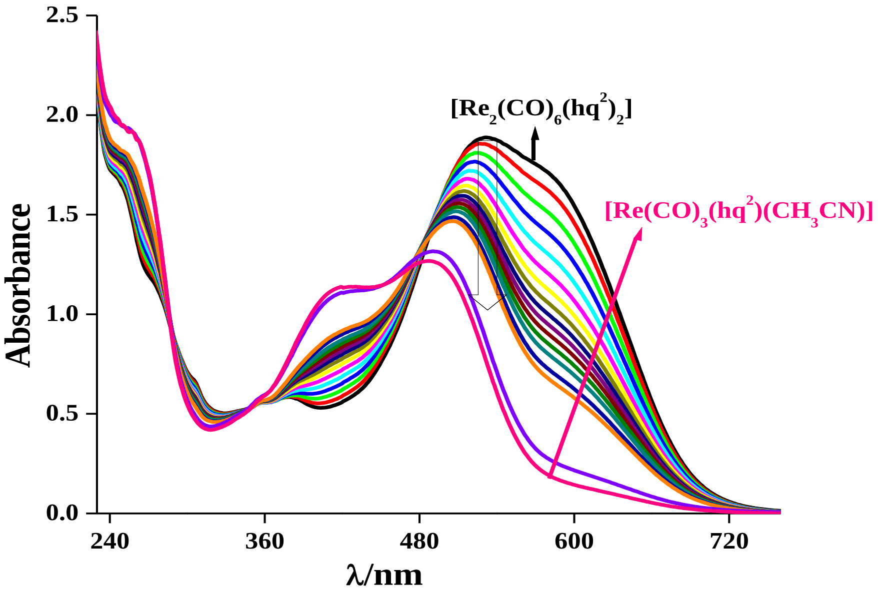

Fig. S15 Time evolution of UV-Vis absorption spectra (recorded at different time intervals) for 4.40 × 10^{-5} (M) solution of [$Re_2(CO)_6(hq^2)_2$], **2** in acetonitrile at room temperature.

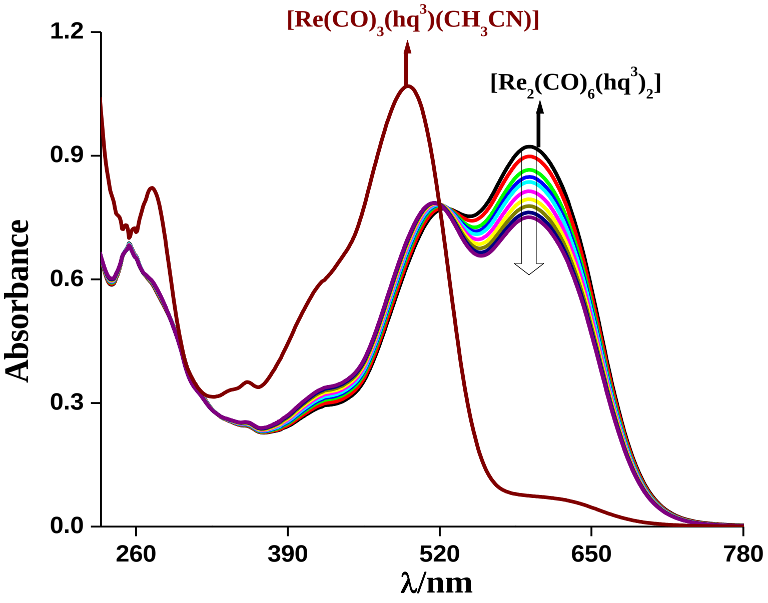

Fig. S16 Time evolution of UV-Vis absorption spectra (recorded at different time intervals) for 3.43 × 10^{-5} (M) solution of [$Re_2(CO)_6(hq^3)_2$], **3** in acetonitrile at room temperature.

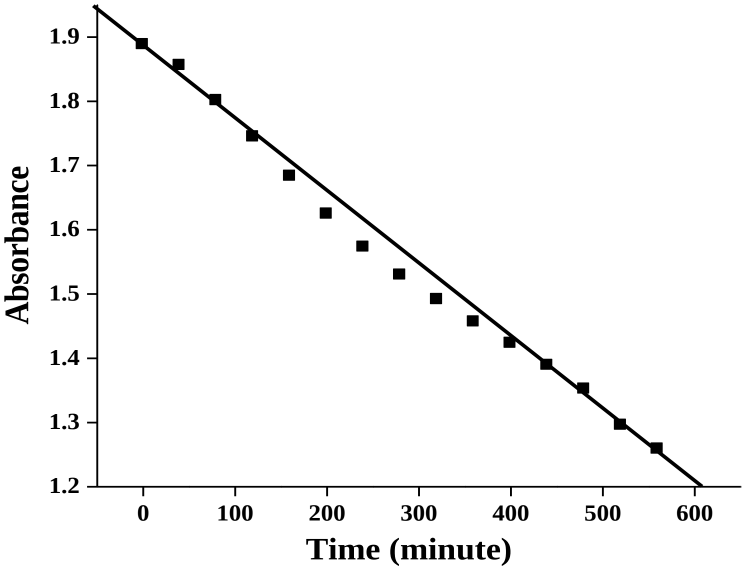

Fig. S17 Absorbance changes (monitored at 531 nm) for 4.40 × 10^{-5} (M) solution of $[Re_2(CO)_6(hq^2)_2]$, **2** in acetonitrile at different time intervals.

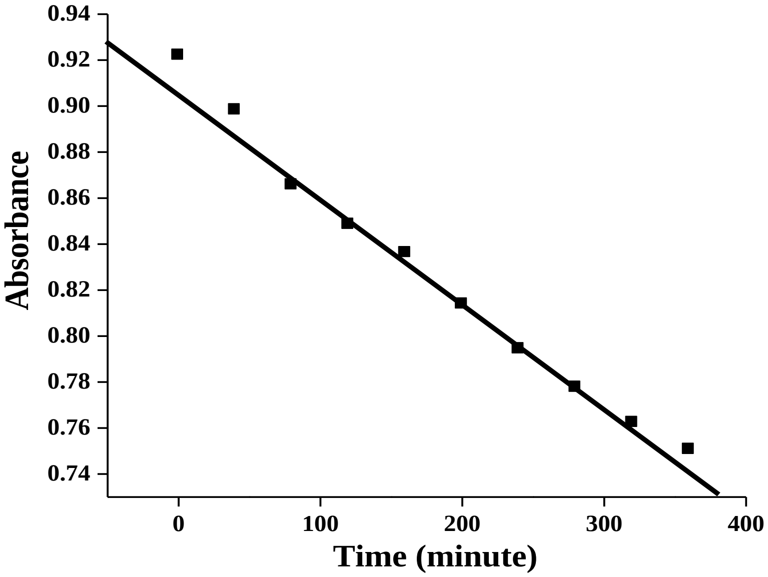

Fig. S18 Absorbance changes (monitored at 596 nm) for 3.43 × 10^{-5} (M) solution of $[Re_2(CO)_6(hq^3)_2]$, **3** in acetonitrile at different time intervals.

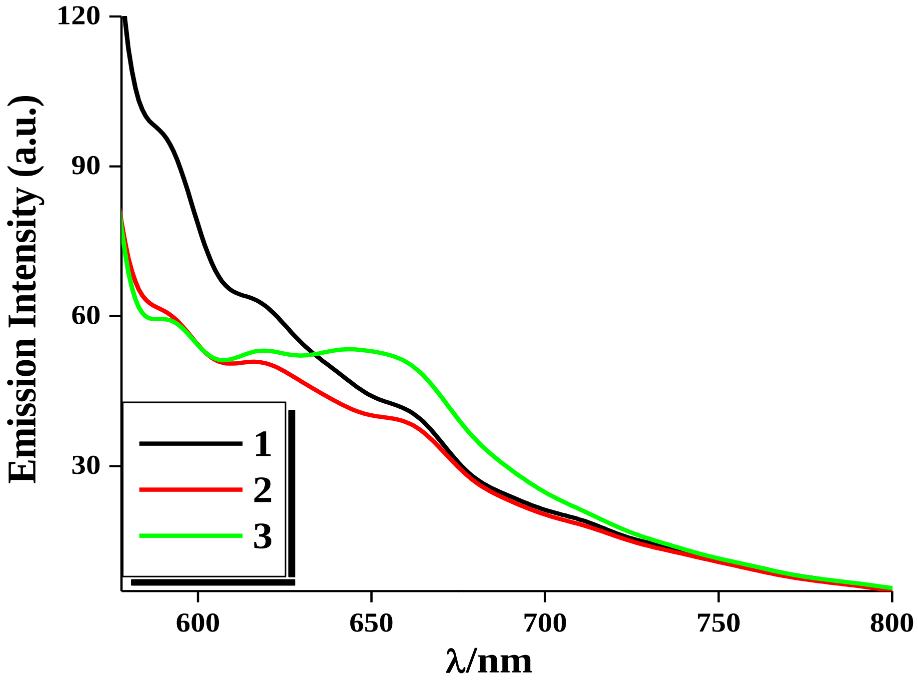

Fig. S19 Emission spectra of dinuclear complexes [$Re_2(CO)_6(hq^1)_2$], **1**; [$Re_2(CO)_6(hq^2)_2$], **2** and [$Re_2(CO)_6(hq^3)_2$], **3** in dichloromethane solution, at room temperature.

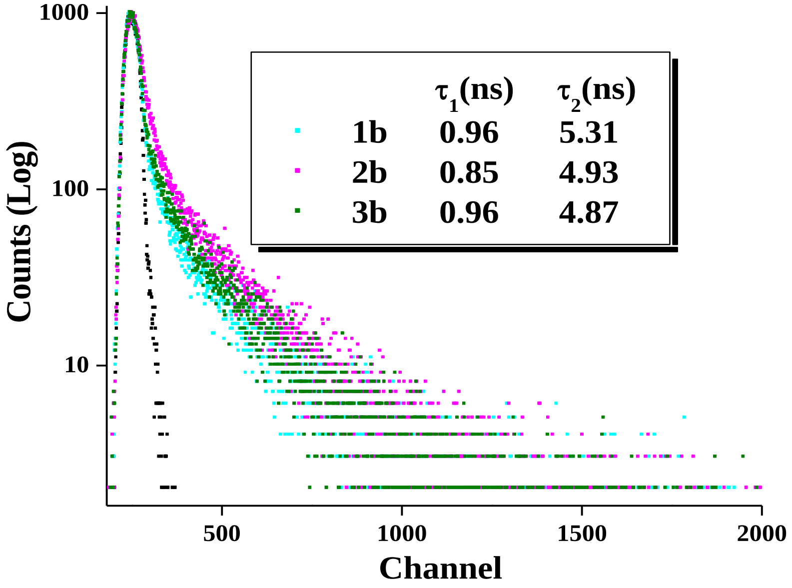

Fig. S20 Changes in the time-resolved photoluminescence decay of complexes [Re(CO)$_3$(hq^1)(N-MeIm)], **1b**; [Re(CO)$_3$(hq^2)(N-MeIm)], **2b** and [Re(CO)$_3$(hq^3)(N-MeIm)], **3b** in CH$_3$CN at room temperature obtained with 450 nm excitation. The emission at 559, 559 and 570 nm was monitored for **1b**, **2b** and **3b**, respectively.

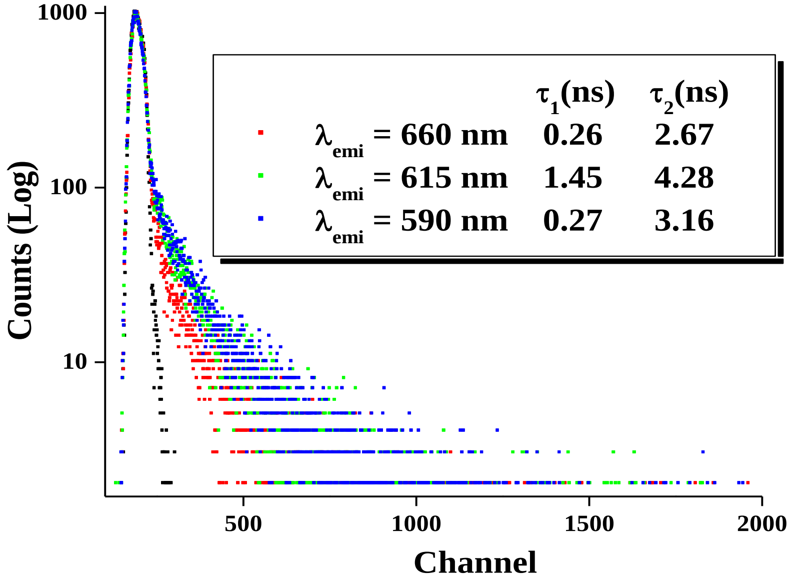

Fig. S21 Changes in the time-resolved photoluminescence decay of [Re$_2$(CO)$_6$(hq^1)$_2$], **1** in CH$_3$CN at room temperature obtained with 450 nm excitation. The emission at 660, 615 and 519 nm was monitored for **1**.

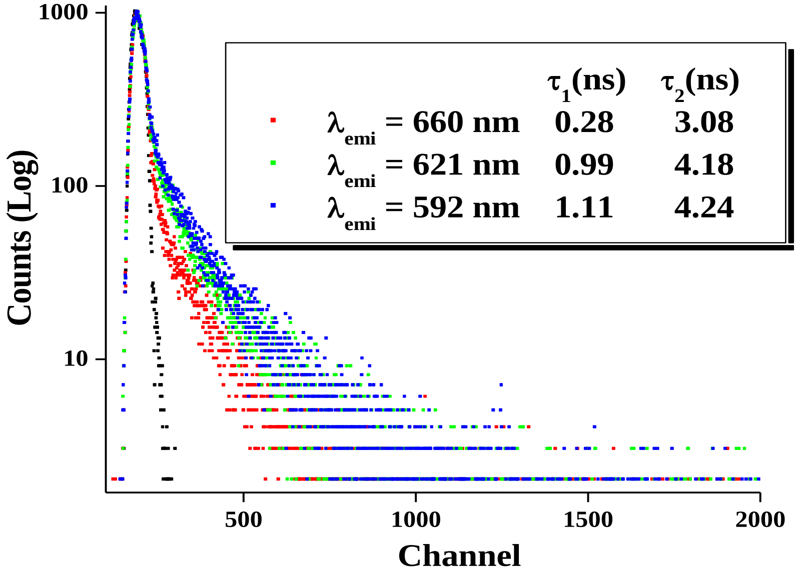

Fig. S22 Changes in the time-resolved photoluminescence decay of $[Re_2(CO)_6(hq^2)_2]$, **2** in CH_3CN at room temperature obtained with 450 nm excitation. The emission at 660, 621 and 592 nm was monitored for **2**.

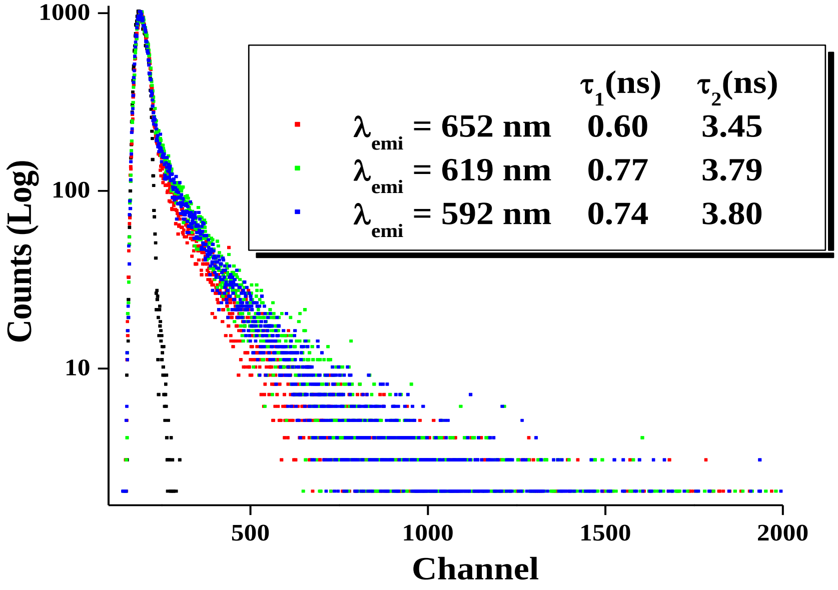

Fig. S23 Changes in the time-resolved photoluminescence decay of $[Re_2(CO)_6(hq^3)_2]$, **2** in CH_3CN at room temperature obtained with 450 nm excitation. The emission at 652, 619 and 592 nm was monitored for **3**.

Table S18 Calculated triplet excited state of $[Re_2(CO)_6(hq^2)_2]$, **2;** $[Re(CO)_3(hq^2)(Im)]$, **2a** and $[Re(CO)_3(hq^2)(N\text{-}MeIm)]$, **2b** in acetonitrile based on the lowest lying triplet state geometry. Main calculated vertical transitions with compositions in terms of molecular orbital contribution of the transition, vertical excitation energies and oscillator strength

Complex	Excitation	Composition	Excitation Energy	Oscillator Strength (f)	CI	Assign	λ_{exp} (nm)
2	1	H – 3 → L	1.8712 eV (662 nm)	0.0255	–0.14929	^{3}ILCT	660
		H – 2 → L + 1			0.14176	^{3}ILCT	
		H – 1 → L + 1			0.50242	^{3}ILCT	
		H → L			–0.49100	^{3}ILCT	
	2	H – 1 → L	2.0512 eV (604 nm)	0.0111	–0.40050	^{3}ILCT	621
		H – 1 → L + 6			0.10790	^{3}ILCT	
		H → L + 1			0.39946	^{3}ILCT	
		H → L + 5			0.11449	^{3}ILCT	
	3	H – 1 → L	2.3182 eV (535 nm)	0.0663	0.31434	^{3}ILCT	592
		H → L + 1			–0.13189	^{3}ILCT	
2a	1	H – 1 → L + 2	2.2261 eV (557 nm)	0.1625	0.23525	^{3}ILCT	559
		H → L + 2			–0.19928	^{3}ILCT	
		H – 1 → L			0.68697	^{3}ILCT	
		H – 1 → L + 1			0.17114	^{3}ILCT	
2b	1	H – 1 → L + 1	2.2271 eV (557 nm)	0.1600	0.17445	^{3}ILCT	559
		H – 1 → L + 2			0.17810	^{3}ILCT	
		H → L + 1			–0.14777	^{3}ILCT	
		H → L + 2			–0.14700	^{3}ILCT	
		H – 1 → L			0.69702	^{3}ILCT	
		H – 1 → L + 1			0.17102	^{3}ILCT	

Table S19 Calculated triplet excited state of [$Re_2(CO)_6(hq^3)_2$], **3;** [$Re(CO)_3(hq^3)$(Im)], **3a and** [$Re(CO)_3(hq^3)$(N-MeIm)], **3b** in acetonitrile based on the lowest lying triplet state geometry. Main calculated vertical transitions with compositions in terms of molecular orbital contribution of the transition, vertical excitation energies and oscillator strength

Complex	Excitation	Composition	Excitation Energy	Oscillator Strength (f)	CI	Assign	λ_{exp} (nm)
3	1	H – 3 → L + 1	1.7918 eV (692 nm)	0.0247	–0.13888	^{3}ILCT	652
		H – 2 → L			0.13897	^{3}ILCT	
		H – 1 → L + 1			–0.54322	^{3}ILCT	
		H → L			0.58081	^{3}ILCT	
	2	H – 1 → L	2.0504 eV (605 nm)	0.0137	–0.34631	^{3}ILCT	619
		H – 1 → L + 6			0.36059	^{3}ILCT	
		H – 1 → L + 1			0.54682	^{3}ILCT	
		H – 16 → L + 1			0.10905	^{3}ILCT	
		H – 17 → L			–0.10086	^{3}ILCT	
	3	H – 1 → L + 1	2.0559 eV (603 nm)	0.0056	0.31323	^{3}ILCT	592
		H → L			–0.37740	^{3}ILCT	
		H – 1 → L			0.55143	^{3}ILCT	
		H – 17 → L + 1			–0.10612	^{3}ILCT	
		H – 16 → L			0.11477	^{3}ILCT	
3a	1	H → L	2.0765 eV (597 nm)	0.0708	–0.33870	^{3}ILCT	571
		H – 1 → L			0.10608	^{3}ILCT	
3b	1	H → L	2.1061 eV (589 nm)	0.0708	–0.31119	^{3}ILCT	570

^{3}ILCT		Hole	Electron
1	w = 0.75 1.9074 eV (0.0095) $\pi \rightarrow \pi^*$ λ_{exp} = 650 nm	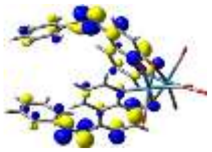	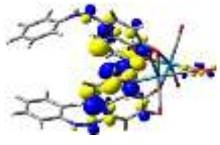
2	w = 0.50 1.8712 eV (0.0255) $\pi \rightarrow \pi^*$ λ_{exp} = 660 nm	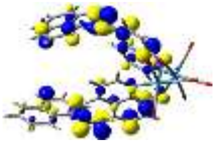	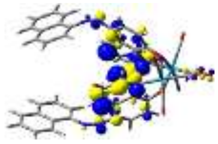
3	w = 0.67 1.7918 eV (0.0247) $\pi \rightarrow \pi^*$ λ_{exp} = 652 nm		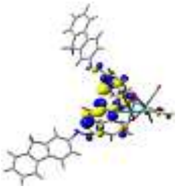
1	w = 0.73 1.9211 eV (0.0056) $\pi \rightarrow \pi^*$ λ_{exp} = 615 nm	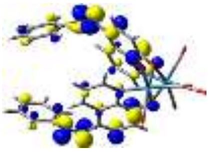	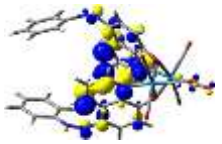
2	w = 0.32 2.0512 eV (0.0111) $\pi \rightarrow \pi^*$ λ_{exp} = 621 nm	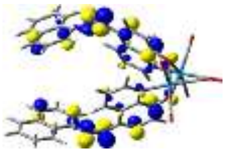	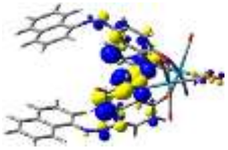
3	w = 0.60 2.0504 eV (0.0137) $\pi \rightarrow \pi^*$ λ_{exp} = 619 nm	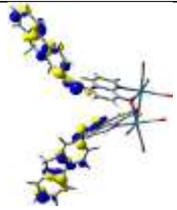	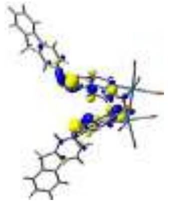
1	w = 0.90 2.3186 eV (0.0119) $\pi \rightarrow \pi^*$ λ_{exp} = 590 nm	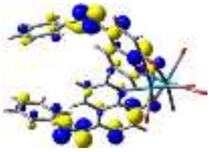	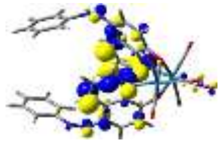
2	w = 0.20 2.3182 eV (0.0663) $\pi \rightarrow \pi^*$ λ_{exp} = 592 nm	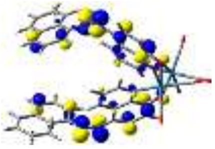	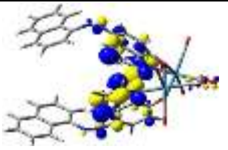
3	w = 0.61 2.0559 eV (0.0056) $\pi \rightarrow \pi^*$ λ_{exp} = 592 nm	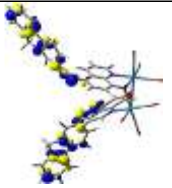	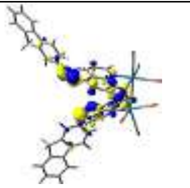

Fig. S24 Natural transition orbitals (NTOs) for the complexes **1**, **2** and **3** illustrating the nature of optically active triplet excited state in their emission bands. For each state, the transition energy (eV), and the oscillator strength (in parentheses) are listed. Shown are only occupied (holes) and unoccupied (electrons) NTO pairs that contribute more than 20% to each excited state. The transition has ^{3}ILCT character: charge is transferred from π hole orbital to the π^*orbital of the ligands.